A HIGH TEMPERATURE STUDY ON THE VAPORIZATION OF ALKALIS FROM MOLTEN BASALTS UNDER HIGH VACUUM: A MODEL FOR LUNAR VOLCANISM

A THESIS SUBMITTED TO THE GRADUATE DIVISION OF THE UNIVERSITY OF HAWAII IN PARTIAL FULFILLMENT OF THE REQUIREMENTS FOR THE DEGREE OF

MASTER OF SCIENCE

IN CHEMISTRY

MAY 1975

By

James Leslie Gooding

Thesis Committee:

David W. Muenow, Chairman
John J. Naughton
Robert W. Buddemeier

We certify that we have read this thesis and that in our opinion it is satisfactory in scope and quality as a thesis for the degree of

Master of Science in Chemistry

THESIS COMMITTEE

David W. Muenow, Chairman

John J. Naughton

Robert W. Buddemeier

TABLE OF CONTENTS

TABLE OF CONTENTS

(Continued)

LIST OF TABLES

LIST OF FIGURES

LIST OF FIGURES

(Continued)

ABSTRACT

Knudsen cell-quadrupole mass spectrometry was used to study the high-temperature vaporization of Hawaiian basalts, plagioclase feldspar, tektites, and samples from the Allende meteorite. Procedures are described by which mass loss rates and vapor pressures of Na and K were measured quantitatively.

Gas-rich glassy basalts were observed to vesiculate under vacuum over the 900-1000°C region and simultaneously evaporate alkalis in nonequilibrium fashion at rates of approximately 200-300 μg Na/g/hr and 75-250 μg K/g/hr. Degassed residues of the same basalts demonstrated equilibrium evaporation rates (over the same temperature range) of 60-120 μg Na/g/hr and 30-60 μg K/g/hr. The gas-deficient plagioclase and tektite samples showed only equilibrium vaporization with rates of 60 μg Na/g/hr, 10 μg K/g/hr (plagioclase) and 10 μg Na/g/hr, 5 μg K/g/hr (tektites) at 900-1000°C. The Allende meteorite vaporized at rates of 2400 μg Na/g/hr and 200 μg K/g/hr at 900-1000°C, possibly by the reaction of alkali oxides with iron sulfide or carbon, or by the thermal decomposition of nepheline or sodalite.

The nonequilibrium vaporization of alkalis from the gas-rich basalts is attributed to vigorous agitation of the melt during its vesiculation by a gas phase composed principally of SO_2, CO_2, H_2O, CO, and H_2S. The major gases released from the Allende meteorite at 900-1000°C are, in order of decreasing abundance, CO, S_2, CO_2, H_2O, SO_2, and H_2S.

It is proposed that nonequilibrium vaporization of alkalis during the vesiculation of lunar lavas was responsible for the production of alkali-rich vapors which subsequently deposited plagioclase crystals in the vugs of lunar rocks. The vesiculative, nonequilibrium vaporization of Na and K during a lunar volcanic eruption should be expected to occur at a high rate upon initial extrusion of the lava into vacuum but then decrease by a factor of approximately three when degassing is completed. Vaporization losses remain inadequate to explain the uniformly low alkali concentrations in lunar basalts.

ACKNOWLEDGEMENTS

I thank my research advisor, Dr. David W. Muenow, for his general guidance and for granting me a very enjoyable degree of freedom in my research efforts.

Dr. John J. Naughton generously shared his materials and ideas and made many helpful comments.

A brief but fruitful discussion with Dr. Klaus Keil aided significantly in my interpretation of results.

John Killingley provided valuable advice on analytical instrumentation.

Virginia A. Lewis graciously conducted atomic absorption spectrophotometric analyses on several rock samples.

Dr. Roy S. Clarke, Jr. of the Smithsonian Institution kindly provided the tektite specimens.

Dr. Robert I. Tilling of the U. S. Geological Survey Hawaiian Volcano Observatory supplied basalt samples and some greatly appreciated encouragement.

I am grateful to the University of Hawaii for financial support.

"We shall not cease from exploration
And the end of all our exploring
Will be to arrive where we started
And know the place for the first time . . ."

-- T. S. Eliot,
Four Quartets

I. INTRODUCTION

A. Statement of Problem

Alkali Deficiencies in Lunar Basaltic Rocks

On July 20, 1969 man made his first direct sampling of another planetary body. That event, the first visit by men to the surface of the Moon, included the collection of rock samples which provided an unprecedented wealth of information about the chemical history of the solar system.

Countless sophisticated chemical investigations have been made on the rocks returned from the six manned lunar landings but the results are not yet fully understood. Only terrestrial rocks and meteorites are presently available for comparison with lunar rocks but the similarities and differences among the three types of material have yielded significant geochemical information.

Lunar rocks may be broadly divided into two general types: the anorthosite-norite-troctolite suite which is common in the lunar highlands, and the mare basalts which fill the large lowland basins. Except where their mention is necessary for completeness, the highland rocks will be largely ignored in this thesis and major emphasis will be placed, instead, on the basaltic rocks of the lunar lowlands.

The data in Table 1 show that terrestrial Hawaiian basalts, lunar mare basalts, and carbonaceous chondrites are chemically similar in some respects but noticeably different

Table 1

A Comparison of the Weight Per Cent Chemical Compositions of Some Terrestrial and Extraterrestrial Rock Materials

	Hawaiian Tholeiitic Basalt (a)	Apollo 12 Olivine Basalts (b)	Allende Carbonaceous Chondrite(c)	Average Australian Tektite(d)
SiO_2	48.43	44.24	34.23	73.06
Al_2O_3	10.89	8.02	3.27	12.57
Fe_2O_3	1.67	0	0	0.60
FeO	9.79	21.22	27.25	4.14
Cr_2O_3	nd	0.63	0.52	nd
MgO	15.47	14.31	24.62	2.04
CaO	8.43	8.54	2.61	3.38
Na_2O	1.89	0.22	0.45	1.27
K_2O	0.40	0.06	0.03	2.20
H_2O^+	0.40	0	0.1	tr
H_2O^-	0.03	0	0	nd
TiO_2	2.16	2.64	0.15	0.68
P_2O_5	0.22	0.08	0.23	nd
MnO	0.17	0.28	0.18	0.12
Cl	0.02	$\leq$ 0.002 (e)	nd	nd
F	0.03	$\leq$ 0.02 (e)	nd	nd
S	0.1	$\leq$ 0.02 (e)	2.06	nd
C	nd	$\leq$ 0.02 (e)	0.29	nd

(a) sample 1699 reported by Moore (1965); designated B1 in this study.
(b) Table 5, Rhodes and Hubbard (1973).
(c) Column 3, Table 3, Clarke, et al. (1970).
(d) Table 4, Schnetzler and Pinson (1962).
(e) Mason and Melson (1970), 116-154.

in other respects. All three materials are rich in iron and magnesium although the lunar basalts and the carbonaceous chondrite contain no Fe(III) as is found in the terrestrial basalt. Virtually no water is present in the lunar basalts although some is contained in the chondrite while the concentrations of sodium and potassium in the same two materials are approximately 3 - 10 times less than those in terrestrial basalts.

With respect to concentrations of water and alkalis, tektites are intermediate between terrestrial and extraterrestrial rocks. They contain exceedingly small amounts of water but possess alkali concentrations which match neither those of terrestrial basalts nor those of lunar basalts and carbonaceous chondrites. The origin of tektites remains unsettled although it is generally assumed that they resulted from meteoritic or cometary impacts on the Earth (Taylor, 1973) or Moon (Chapman and Larson, 1963). However, the differences in composition between lunar rocks and tektites have created a serious difficulty for the lunar hypothesis of tektite origin (Taylor, 1973).

A substantial amount of debate has centered on whether the low-alkali character of lunar mare basalts is of primary or secondary origin. Many workers have concluded that the alkali deficiency is a primary feature, reflecting the petrogenesis of lunar basalts from source materials poor in alkalis (Ringwood and Essene, 1970; Gast, et al., 1970; Rhodes and Hubbard, 1973), perhaps as the result of chemical

fractionation during the accretion of the Moon (Anderson, 1973). Others have argued that the low alkali concentrations in lunar basalts are of secondary origin, the result of vaporization losses which occurred upon the extrusion of the lavas into the high vacuum environment of the lunar surface (O'Hara, et al., 1970; Biggar, et al., 1971).

Understanding the chemical history of the Moon is crucial to our understanding of the history of the solar system. The importance of vaporization effects must be determined before realistic models for the evolution of terrestrial planets can be constructed. Thus, the objective of the research described in this thesis was to test the hypothesis of secondary origin for the alkali deficiency in lunar mare basalts. The use of Hawaiian basalts as sample materials in the high temperature, high vacuum simulation of a lunar lava flow should permit evaluation of the usefulness of the vacuum vaporization hypothesis in explaining the alkali deficiencies in lunar basalts. Similar studies of tektites and the Allende carbonaceous chondrite might elucidate their possible petrogenetic relationships to lunar basalts.

B. Investigational Approach

1. Summary of Previous Work

Vacuum vaporization studies of lunar samples have been conducted by many workers (De Maria, et al., 1971; Gibson and Hubbard, 1972; Gibson and Johnson, 1971; Naughton, et al., 1971) but, while the high temperature vaporization of sodium

and potassium was observed, the results were interpreted as being insufficient to explain the uniformly low alkali concentrations in lunar materials (Gibson and Johnson, 1971). Storey (1973), however, offered as evidence to the contrary the alkali losses measured for the vacuum fusion of a terrestrial basalt. Thus, the importance of vacuum vaporization in controlling the compositions of lunar lavas has yet to be conclusively demonstrated.

Evidence exists, though, to support the occurrence of alkali metal metal mobilization events on the lunar surface. Naughton, et al. (1972) predicted that alkali species should be abundant in the vapor clouds formed during lunar volcanic eruptions and impact events and presented evidence (Naughton, et al., 1971) that the subsequent condensation of such alkali vapors might result in the chemical erosion of lunar surface rocks.

Brown and Peckett (1971) proposed that vaporization losses of alkalis from the melt were responsible for the apparent reverse compositional zoning of the plagioclase crystals in lunar rock 14310. Brown, et al. (1972) similarly proposed that the variable alkali concentrations in the residual glasses of individual lunar basalt samples were the result of vaporization effects which operated during the formation of the rocks. More direct evidence for the movement of metallic vapors across the lunar surface is based on the occurrence of filamentary microcrystalline "whiskers" on the surfaces and vuggy interiors of some lunar materials.

Such whiskers were found among the dust particles which coated the camera lens of the Surveyor 3 spacecraft (Brownlee, et al., 1972) and on the vesicle walls of lunar basalts (Skinner and Winchell, 1972). Similar whisker-like crystals were later discovered on the surfaces of lunar breccias (Carter, 1973) and among samples of lunar fines (Jedwab, 1973). The morphologies of the crystalline whiskers suggested that they grew from the vapor phase. The lunar whiskers exhibited a range of compositions including phases rich in iron, sulfur, and titanium but those discovered in the vesicles of basalts by Skinner and Winchell (1972) were determined to be a type of plagioclase rich in sodium and potassium.

It seems probable, then, that the vapor phase movement of alkali metals and other volatile species has occurred at various times throughout lunar history. However, important questions concerning the mechanisms and effects of such vapor phase transport events have not been answered.

Previous investigations have typically used mass spectrometry to study the vaporization of lunar basalts (Gibson and Hubbard, 1972) or atomic absorption spectrophotometry to determine the alkali concentrations in the residues of basalts which have been subjected to vacuum fusion (Storey, 1973). The two complementary techniques have provided useful information but have not been applied to a sufficient number of basalts of either terrestrial or lunar origin to yield conclusive results concerning the question of alkali

vaporization during lunar volcanism. In particular, the characterization of the vaporized alkalis and the mechanisms of their formation have not been fully explored.

2. Experimental Plan

In an attempt to gain further understanding of the vaporization effects to be expected during lunar volcanic eruptions, the techniques of high temperature mass spectrometry were applied to the study of the vaporization behavior of terrestrial basalts under high vacuum, with particular emphasis on characterizing the vesiculation process. The important differences between this study and previous related investigations include the sophistication and mode of operation of the instrumentation, the analytical procedures, and the selection of samples used for analysis.

The Knudsen cell-quadrupole mass spectrometer system which was used in this study possessed a number of unique features which were not employed by previous investigators (see pages 18-24). Such features were crucial to the recognition of the vaporization effects described in this thesis and may partly explain the inability of previous workers to discern such effects.

Another important disctinction between this and previous studies were the samples which were selected for study and which are described in Table 2. Since glassy rocks should more closely resemble the physical-chemical state of molten lava than would holocrystalline rocks,

Table 2

Description of Samples*

Sample	Description
B1	Submarine basalt from E. rift zone of Kilauea volcano, Hawaii. Sample 1699 as described by Moore (1965). Vitrophyric. Mode: 66 gl, 22 ol, 6 px, 6 pl. (2% vesicles).
B2	Submarine basalt from E. rift zone of Kilauea volcano, Hawaii. Sample 1712 as described by Moore (1965). Vitrophyric. Mode: 81 gl, 14 ol, 3 px, 2 pl. (1% vesicles).
B3	Subaerial basaltic spatter erupted and collected May 5, 1973, Pauahi-Hiiaka flow, Kilauea volcano, Hawaii. USGS Hawaiian Volcano Observatory sample no. PH573-3. Vitrophyric. Mode: 95 gl, 5 ol. (50% vesicles).
B4	Subaerial basaltic spatter erupted and collected September 25, 1971, upper SW rift zone of Kilauea volcano, Hawaii. Vitrophyric. Mode: 90 gl, 5 ol, 5 pl. (75% vesicles).
P	Plagioclase feldspar (An_{78} from chemical analysis) separated from a feldsparphyric basalt collected near Molukeia, Upper Waianae Range, Oahu, Hawaii.
T1	Phillipine tektite. Smithsonian Institution sample no. NMNH-1912.
T2	Australian tektite. Smithsonian Institution sample no. NMNH-2302.
M	Allende carbonaceous chondrite. Described by Clarke, et al. (1970).

*The approximate modal analyses are given on a vesicle-free basis as percent glass (gl), olivine (ol), pyroxene (px), and plagioclase (pl). The values for percent vesicles are from Moore (1965) and visual estimates made in this study.

the samples chosen as starting materials were fresh, well-documented Hawaiian basalts which had been rapidly quenched either subaqueously (B1, B2) or subaerially (B3, B4). It was hoped that samples of the attendant volatile phases had been preserved in the quenched lavas such that vesiculation could then be observed during their re-melting under high vacuum. The submarine basalts (B1, B2) were chosen specifically for their expected high gas contents. Because B1 and B2 have been shown to be essentially unaltered and free of significant sea water contamination (Moore, 1965; Hart, 1973) and since B3 and B4 were collected immediately after eruption, the four basalts represent the freshest examples of their respective types which could be obtained.

The descriptions of samples P, T1, T2, and M given in Table 2 are self-explanatory. P was included so that the vaporization behavior of the molten basalts could be compared with that of an alkali-rich crystalline phase which serves as a major repository for sodium and potassium in crystalline basalts. T1 and T2 were selected as examples of natural silicate glasses having alkali concentrations comparable to or greater than those in B1-B4 but which contained much less gas than the latter set of materials (Friedman, 1963). Finally, M was chosen because its alkali concentrations were similar to those of lunar mare basalts (see Table 1) and because it contained abundant C, S, and Cl which were expected to form gases under the planned experimental conditions. In addition, sample M may be

chemically similar to the source material of lunar basalts since certain of its chondrules have been suggested as representative of the condensate which formed the Moon (Anderson, 1973).

The general experimental plan was to determine the vaporization behavior of each type of sample material under high vacuum at temperatures which were typical of molten basalts, namely, 1000-1200° C. The vapor species released from the samples were to be identified by mass spectrometry with particular emphasis being placed on study of the vesiculation process and characterization of the mechanisms of alkali vaporization from basalts. By quantitatively determining the rates of alkali vaporization from the different samples it was hoped that information could be gathered which would permit evaluation of the importance of vaporization effects in controlling the alkali concentrations in lunar mare lavas.

II. EXPERIMENTAL PROCEDURE

A. Theory of Knudsen Cell-Quadrupole Mass Spectrometry

The coupling of a Knudsen cell with a mass spectrometer provides a powerful analytical arrangement for the study of vaporization processes at high temperatures. If the conditions for Knudsen vaporization (Knudsen, 1908) are achieved a sample of the equilibrium vapor above a solid at a given temperature can be formed into a molecular beam and delivered to the ion source of a mass spectrometer which then facilitates rapid identification of the chemical species which are present in the beam. The general techniques for high temperature mass spectrometry are well known and have been reviewed by Grimley (1967) and by Drowart and Goldfinger (1967).

High temperature mass spectrometry using a quadrupole mass filter has several unique features and advantages which stem from the principles of quadrupole filter operation, the theory of which has been reviewed by Dawson and Whetten (1969). Basically, an ion of mass-to-charge ratio m/e is directed along the axis of a quadrupole electric field comprised of a DC voltage, U, and an RF voltage, V. The potential, Φ, at any point in the field is given in rectangular coordinates as

$$\Phi = (U - V\cos \omega t)(\lambda x^2 + \sigma y^2 + \gamma z^2) \qquad (1)$$

where ω is the angular frequency of the applied RF field, t is the time in seconds, and λ, σ, and γ are constants.

The electric field, E, at point (x, y, z) exerts a force of $eE = m(d^2i/dt^2)$ on the entering ion of mass m and charge e, forcing it to accelerate at rate d^2i/dt^2 in the direction i. The resultant motion of the ion can be resolved into x, y, and z components as

$$\frac{d^2u}{dt^2} + \left(\frac{e}{m}\right)(U - V\cos\omega t)(2\, c_u t) = 0 \qquad (2)$$

where u = x, y, or z and $c_u = \lambda$, σ, or γ, respectively. Generally, though, the geometry of the field of radius r_o is chosen so that $\gamma = 0$, thereby reducing the problem to one of two-dimensional motion in the xy plane.

By defining

$$\omega t = 2\xi, \quad a = \frac{4eU}{mr_o^2\omega^2}, \quad q = \frac{2eV}{mr_o^2\omega^2} \qquad (3)$$

Equation (2) can be rewritten in the form

$$\frac{d^2u}{d\xi^2} + (a - 2q\cos 2\xi)u = 0 \qquad (4)$$

which is known as the Mathieu equation. Solutions to Equation (4) give stable trajectories for certain values of a and q. For an ion to successfully pass through the quadrupole mass filter it must have stable trajectories in both the x and y directions. The (a, q) stability domain which

is ordinarily used in quadrupole mass spectrometry is shown in Figure 1. An infinite number of straight lines of constant a/q ratio can be drawn from the origin through the stable trajectory region. Such lines are called "scan lines" since, by Equations (3), $a/q = 2U/V$ represents a path by which the quadrupole field components, U and V, can be varied to produce a continuum of stable trajectories, each of which is uniquely favorable to an ion having a certain m/e ratio. Thus, as U and V are varied under the condition $2U/V$ = constant, ions of successively smaller m/e ratio are passed through the mass filter as a and q increase proportionally from the origin in Figure 1. The mass spectrum is thereby scanned.

The quadrupole mass filter has the advantage of small size compared to mass analyzers of the magnetic or time-of-flight varieties, resulting in its greater flexibility in placement relative to the Knudsen cell assembly. Its fast scanning ability makes it preferable to magnetic instruments while its comparatively simple electronic control requirements make it more attractive than time-of-flight instruments.

The detection systems used with quadrupole mass filters are generally the same as those used with other types of mass analyzers.

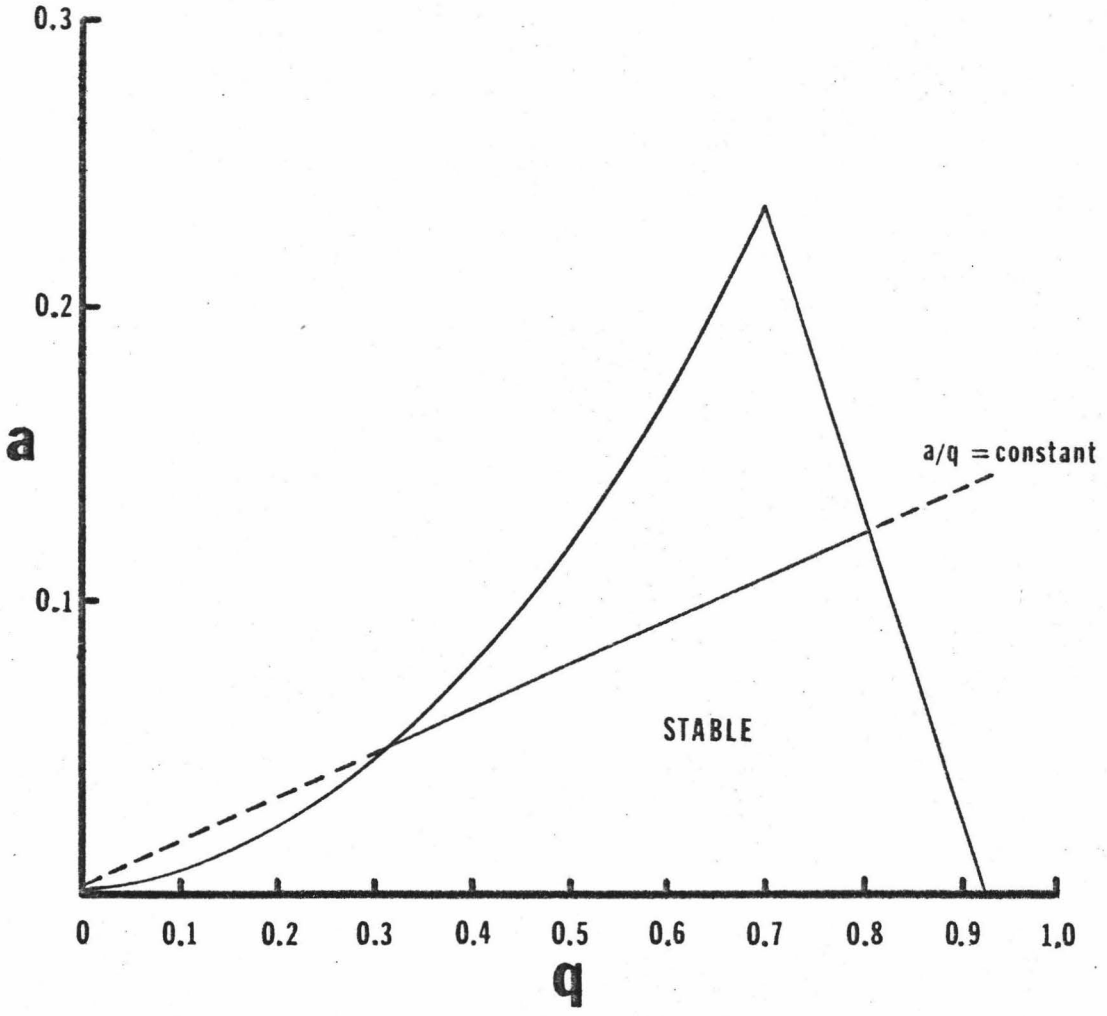

FIGURE 1 The a/q Stability Domain for the Operation of a Quadrupole Mass Filter (after Dawson and Whetten, 1969).

B. Instrumentation

1. General Description

The experimental arrangement used in this investigation is shown schematically in Figure 2. Basically, the apparatus consists of a conventional Knudsen cell assembly and a QUAD® 1110 quadrupole mass filter (Electronic Associates, Inc., Palo Alto, Calif.) which were both housed inside a Varian 934-11110A vacuum system (Varian Associates, Palo Alto, Calif.). The apparatus was assembled largely by Killingley (1975). Detailed instructions for its operation are given in the Appendix.

The pumping system consisted of a mechanical forepump (Welch Duo-Seal Model No. 1402), a titanium sublimation pump (Varian Model No. 916-0017), and an ion pump (Varian VacIon Model No. 912-7001). Under normal conditions the pumping system could achieve a working vacuum of 1×10^{-8} torr. The vacuum housing, shown in Figure 3, consisted of a stainless stell bell jar with numerous flanged ports which facilitated the attachment of various components for the Knudsen cell, mass filter, and detector systems. The bell jar was seated on a fixed base by means of a reusable Viton gasket which permitted convenient access to the bell jar interior for sample introduction and maintenance work. The exterior of the bell jar around the perimeter of the Viton seal was enclosed in a plastic glove bag which was inflated with high-purity nitrogen during the opening of the bell jar for sample introduction and retrieval.

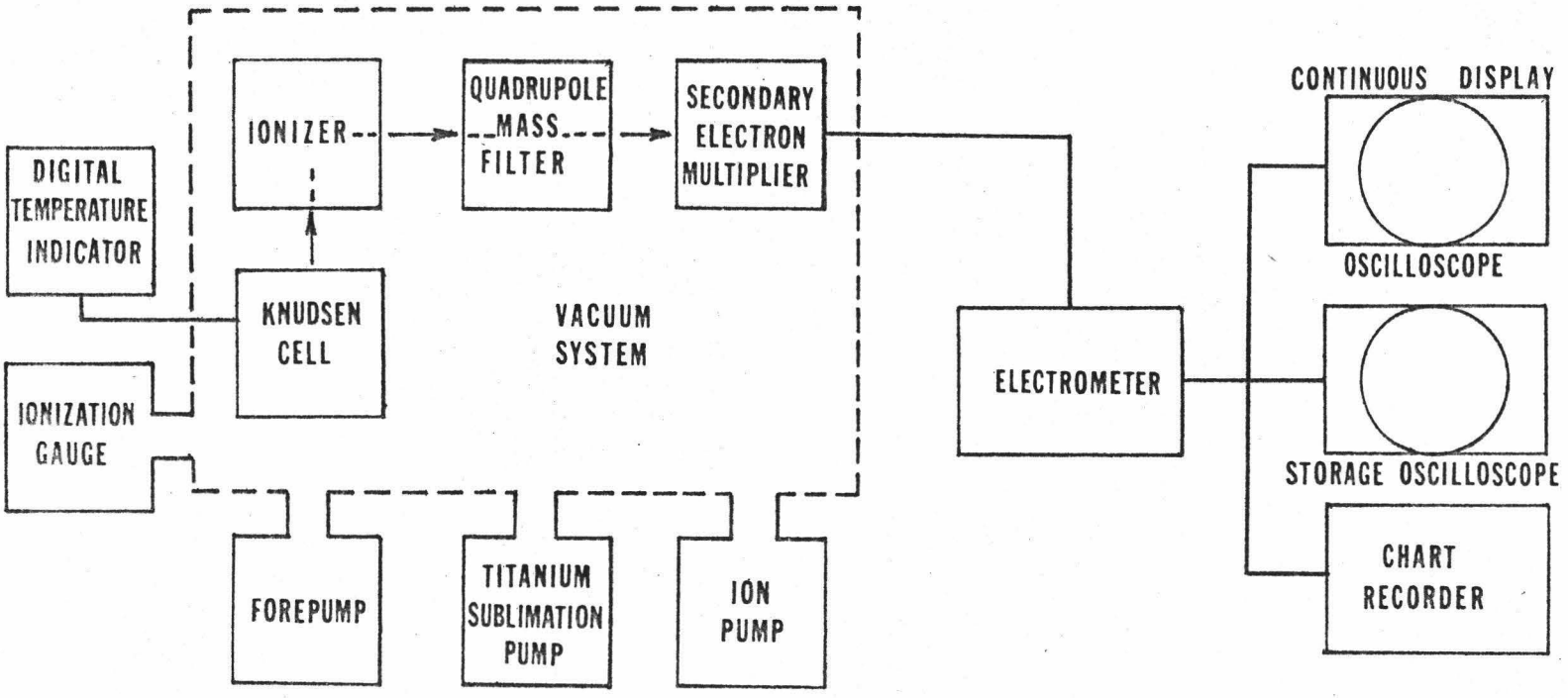

FIGURE 2 Block Diagram of the Quadrupole Mass Spectrometer System.

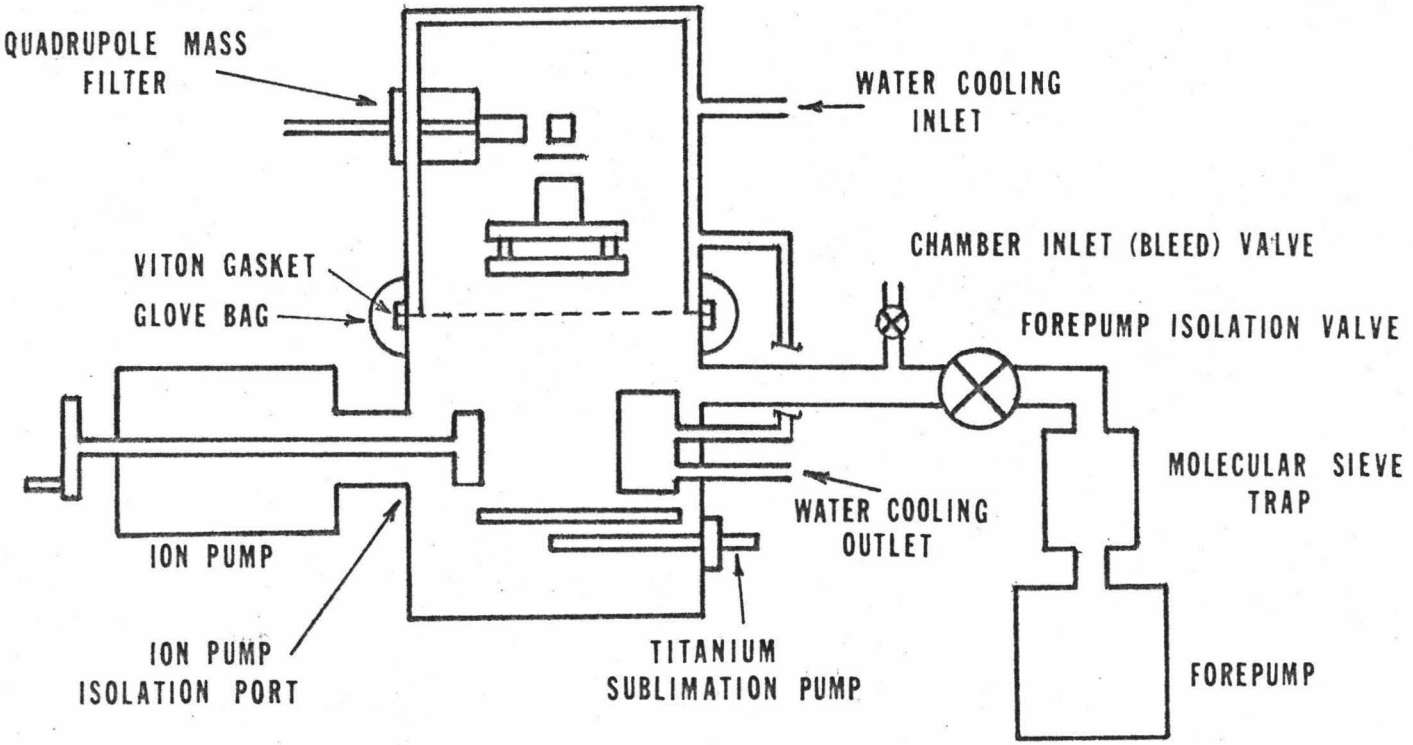

FIGURE 3 Schematic of the Mass Spectrometer Vacuum System.

A water cooling system was contained in the wall structure of the bell jar and was supplemented by a cooling panel near the titanium sublimation pump in the lower half of the vacuum housing.

2. High Temperature Assembly

The Knudsen cell and supporting apparatus, which have been described in detail by Muenow (1973), are shown in Figures 4 and 5. The Knudsen effusion cell, A, was machined from tantalum and surrounded by four coaxial, cylindrical molybdenum heat shields, B. The cell was supported by three tungsten rods, the entire cell/shield combination being held on an adjustable stainless steel positioning plate, C. Heating of the cell was accomplished by radiation from a tantalum resistance element which was supported by two tungsten rods, D. Temperatures were measured by a Pt/Pt-10% Rh thermocouple, E, which was peened into the base of the cell and which was connected externally to a digital temperature indicator (Model No. 2600SC, Newport Laboratories, Inc., Santa Ana, Calif.). The digital indicator registered temperatures which agreed to $\pm$ 5° C with those measured for the same thermocouple by a manually operated precision potentiometer in the range 25-1300° C. The thermocouple temperatures agreed satisfactorily with those measured by optical pyrometry.

A precision feedthrough from the bell jar exterior to the evacuated interior permitted the movement of a shutter-plate, F, between the cell and the ion source. The shutter-

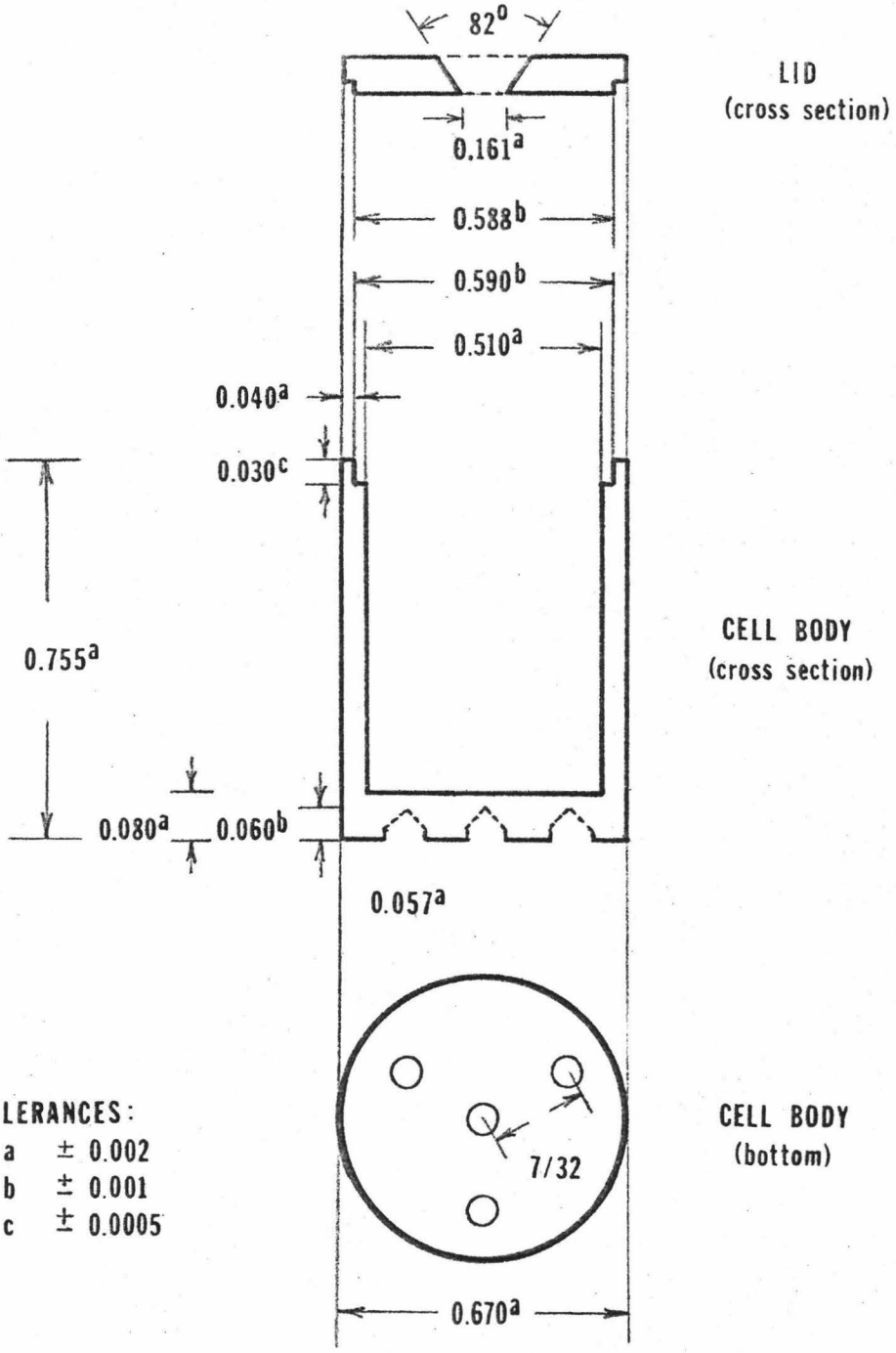

FIGURE 4 Schematic of the Knudsen Cell.
(Dimensions are in inches)

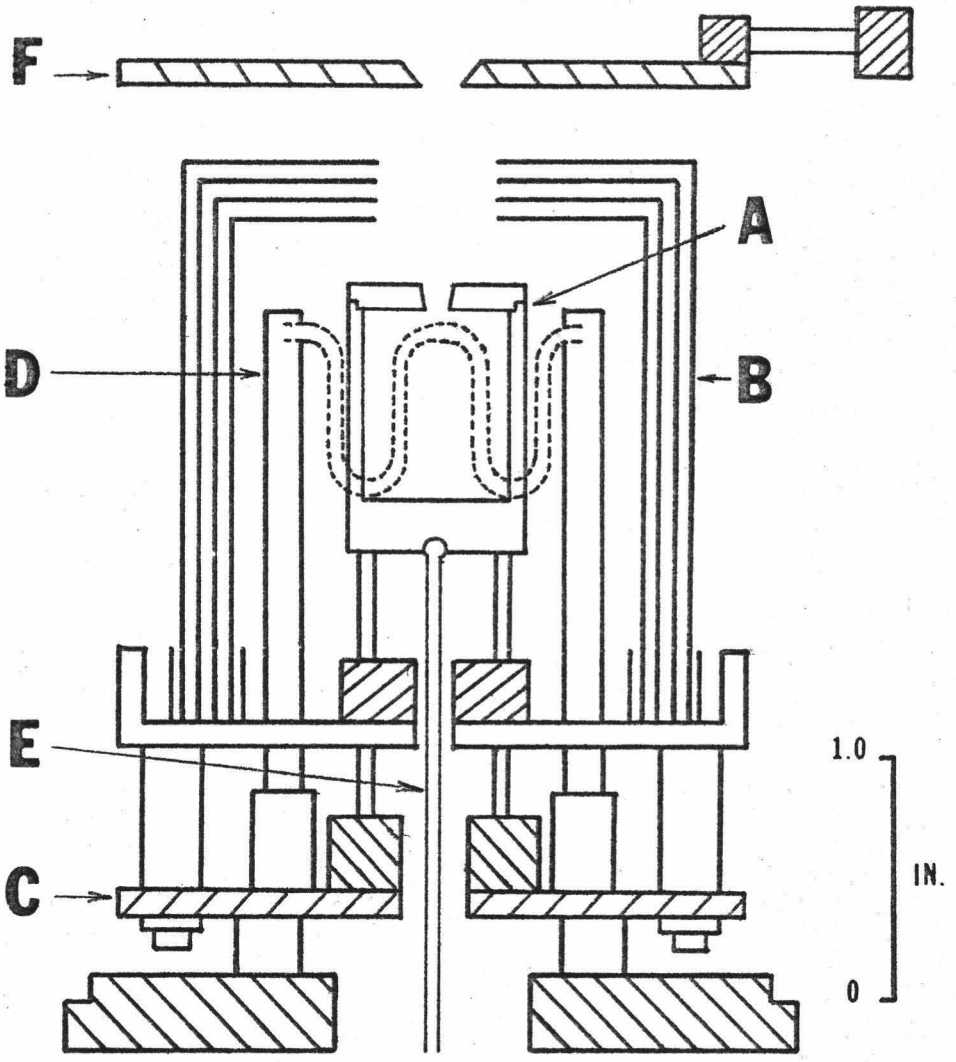

FIGURE 5 Schematic of the High Temperature Assembly (Adapted from Muenow, 1973). The components are the Knudsen cell (A), heat shields (B), positioning plate (C), resistance heating element (D), thermocouple (E), and shutter-plate (F).

plate could be moved across the path of the sample molecular beam and was therefore useful in distinguishing species effusing from the sample-cell from those contributed by background sources.

To minimize reaction between the sample and cell materials at high temperatures, all samples were held in high-purity Lucalox® (99.9% Al_2O_3) cups which were manufactured expressly for the purposes reported here by the Lamp Glass Department of the General Electric Company, Cleveland, Ohio. Each liner cup, as shown schematically in Figure 6, was constructed to slip-fit into the Knudsen cell and was equipped with a precision fitted lid with an orifice.

After use, the Lucalox liner cups and lids were placed in a bath of analytical reagent grade hydrofluoric acid (48% HF) to dissolve any silicate sample residues. They were then soaked in tap water for several hours, subjected to sonic cleaning in a water medium for 1 - 2 hr, and then rinsed in de-ionized water. Before use in further sample work, each liner/lid combination was heated in vacuum to 1300° C (or higher as required) to accomplish desorption and degassing of contaminants.

3. Mass Filter and Detection Systems

The quadrupole mass filter provided analytical capability for ions over the m/e = 2 - 300 range. It was constructed exclusively of stainless steel, alumina, and tungsten so that background contributions were minimized.

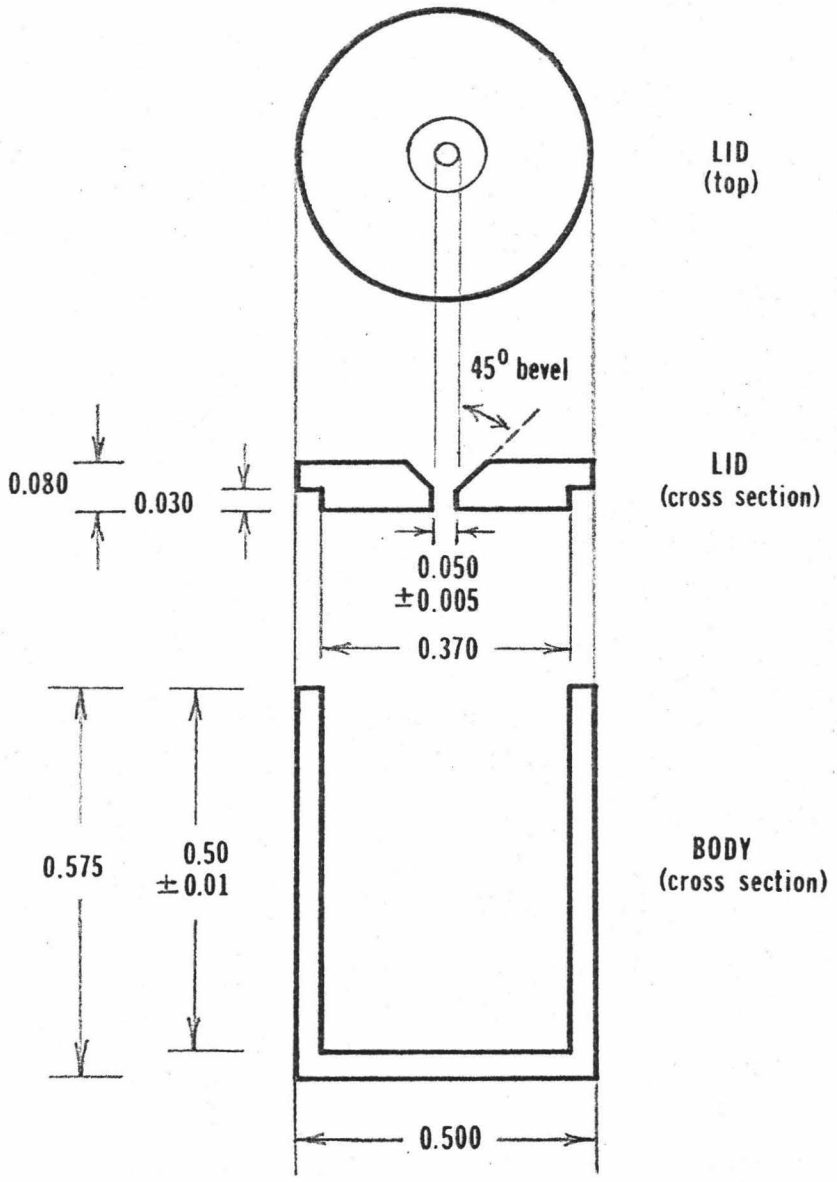

TOLERANCES:
±0.003
except where noted

FIGURE 6 Schematic of Knudsen Cell Lucalox® Liner Cup. (Dimensions are in inches)

The supporting electronic controls were comprised entirely of solid state components. Voltages were supplied to the rods of the mass filter by an RF generator with a 0 - 2400 V ramp at 2.5 MHz and a DC generator with a 0 - 200 V ramp which operated in three linearized stages and which provided positive and negative voltages, respectively, to the two sets of rods. The RF and DC voltages operated in the fixed ratio of U/V = 1/6 such that a/q = 0.33 (c.f. page 13).

The mass filter was capable of scan rates of 0.1, 0.3, 1, 10, 30, 60, 150, 300, 450, 600, and 900 sec per scan although the 30 and 60 rates were used most frequently in the work described here. In addition, the scan generator could be deactivated so that any detectable mass peak could be monitored continuously.

The electron impact ion source was contructed of stainless steel and alumina and utilized a geometry which placed the molecular beam, electron beam, and ion beam in mutually perpendicular orientations. The ionization beam was generated as a sheet of electrons from a 0.006 inch thick tungsten filament which carried a current of 100 μA to 3 mA. The electron energy was fixed at 70 V with an ion accelerating energy of +8 V.

The detection system included both a Faraday collector and a 14-stage copper-beryllium secondary electron multiplier (S. E. M.) although the S. E. M. was used for all measurements included in this report. The first dynode

of the S. E. M. was operated at a potential of -3 kV with respect to ground.

The signal from the S. E. M. was fed to an electrometer (ESA Model 75A, Electronic Associates, Inc.) which in turn fed two oscilloscopes and a chart recorder. The first oscilloscope, which was part of the QUAD® 1110 control unit, was used for continuous display of the mass spectrum in the range of interest while the second oscilloscope, a storage type (Tektronix, Type RM564) was used to observe the "spiking" behavior of certain mass peaks as will be explained later. All analytical data were recorded on a strip chart recorder (Texas Instruments Model No. FS01W6D).

C. Analytical Techniques

1. Mass Spectral Scanning Surveys

As a first step in establishing the vaporization behavior of a given sample material, a small portion (100 - 300 mg) of the sample was heated in the Knudsen cell at 5 - 10° °C/min as the desired mass ranges were scanned at intervals of 25 - 50° C. For the samples used in this investigation the mass range of principal interest was m/e = 4 - 70 which could be conveniently scanned and recorded in 60 sec.

A typical scan of the m/e = 4 - 70 range is shown in Figure 7. Figure 7a is a scan taken with the shutter-plate in the open position while Figure 7b is a scan taken with the

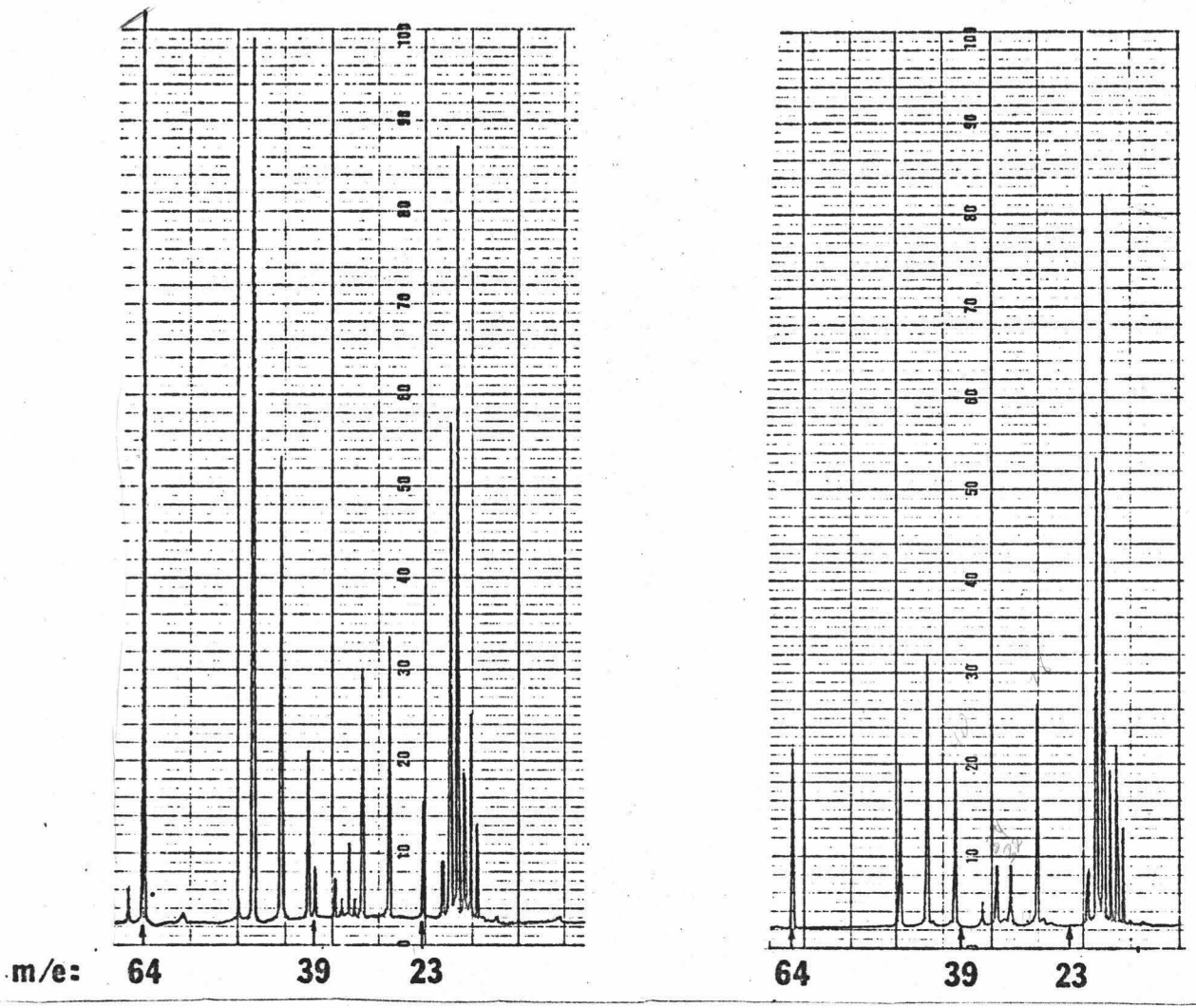

FIGURE 7 Mass Spectrum for Basalt B1 at 950° C.
The spectrum was obtained with
(a) the shutter-plate open and
(b) the shutter-plate closed.

shutter-plate in the closed position, i. e. blocking the sample molecular beam.

Species in the sample beam were identified by their fragmentation patterns and isotopic peaks. Ion intensities were obtained by subtracting the intensities for previous blank runs from those observed in the sample run. Ion intensities for condensible vapors (Na, K, etc.) were obtained for each specie by subtracting the nonshutterable portion of its signal from its total signal in the sample spectrum. Blank runs were used to verify that the background signals at the mass numbers corresponding to the condensible species were indeed nonshutterable.

After the general vaporization behavior of a particular sample had been established, fresh specimens were used in the detailed investigation of the mass and temperature ranges of special interest. All experiments performed in this investigation utilized specimens which were from the interior portions of the rock samples (at least 5 mm beneath identifiable outer surfaces) and which were taken in the form of whole-rock aliquots (individual 5-10 mm chips) except where noted otherwise.

2. Measurement of Alkali Vaporization Rates

The principles of quantitaive analysis by Knudsen cell-mass spectrometry have been reviewed by Grimley (1967). A mass peak, i, is monitored as a function of time such that the number of molecules, Z_i, which are vaporized

during a time interval, $t_2 - t_1$, is given by

$$Z_i = K_i \int_{t_1}^{t_2} I_i^+ \bar{c}_i \, dt \tag{5}$$

where I_i^+ is the measured ion-current intensity, $\bar{c}_i$ is the average molecular velocity, and K_i is the instrumental sensitivity factor. Making the substitution $\bar{c}_i = (8RT/\pi M_i)^{\frac{1}{2}}$, for a specie of molecular weight M_i at cell temperature T gives

$$Z_i = K_i \left(\frac{8R}{\pi M_i}\right)^{\frac{1}{2}} \int_{t_1}^{t_2} I_i^+ T^{\frac{1}{2}} \, dt \tag{6}$$

By defining

$$A_i = \int_{t_1}^{t_2} I_i^+ T^{\frac{1}{2}} \, dt \tag{7}$$

Equation (6) reduces to

$$Z_i = K_i \left(\frac{8R}{\pi M_i}\right)^{\frac{1}{2}} A_i \tag{8}$$

For the sum of measurements over several consecutive time intervals it follows that

$$Z_{i,\,\text{total}} = K_i \left(\frac{8R}{\pi M_i}\right)^{\frac{1}{2}} \sum A_i \tag{9}$$

The total mass of specie i which is vaporized, $W_{i,total}$, is found by multiplying $Z_{i,total}$ by Avogadro's number, N_A, to give

$$W_{i,total} = N_A K_i \left(\frac{8R}{\pi M_i}\right)^{\frac{1}{2}} \sum A_i \qquad (10)$$

Experimentally, the amount of alkali vaporized from a sample at high temperature was measured by monitoring the appropriate mass peak (m/e = 23 for Na, m/e = 39 for K) as a function of time. The possibility of an interference in the potassium analyses existed since the ions K^+ and NaO^+ both appear at m/e = 39 and are indistinguishable without high-resolution or appearance potential measurements. Accordingly, a sample of Na_2O (formed by the thermal decomposition of Na_2CO_3 under vacuum) was vaporized in the Knudsen cell-mass spectrometer system. Decomposition of the Na_2O gave a base peak at m/e = 23 (Na^+) with negligible peaks at 39 (NaO^+) and 62 (Na_2O^+). Furthermore, the absence of substantial m/e = 55 (KO^+) from the mass spectra for the basalts and other samples suggests that its analog, NaO^+, was not an important vapor specie in these experiments. Thus, m/e = 23 and 39 were assumed to correspond to Na^+ and K^+, respectively, in the mass spectrometric analyses performed in this investigation.

During the analytical runs, temperature was also a function of time since heating was continued at a steady rate (5° C/min). The type of data display which was

obtained by the mass peak monitoring procedure is represented schematically in Figure 8. The peak height, H, increased with T during the elapsed time of analysis, $\Delta t = t_f - t_o$. Points Y and Y' show the effect of manually controlled changes in the recorder attenuation which were used to keep signal H on scale. Regions X and X' are places in the analysis where the moveable shutter-plate was used to block the sample beam emerging from the Knudsen cell. Since blank runs repeatedly showed that the m/e = 23 and 39 background signals were nonshutterable, the baseline of the trace was defined during analysis by straight line segments such as XX'.

The recorder trace for each analysis was divided into several trapezoidal sections such as area A in Figure 8. The ion-current, I_i^+, for the analytical specie was related to the peak height, H_i, as

$$I_i^+ = f_i H_i \qquad (11)$$

where f_i is a conversion factor which was calculated from several parameters which will be discussed shortly (see page 31 and Appendix B). Thus, by defining the average quantities $I_i^+ = \frac{1}{2} f_i(H_1 + H_2)$ and $T = \frac{1}{2}(T_1 + T_2)$ the integral in Equation (7) was approximated as $A_i = I_i^+ T^{\frac{1}{2}}(t_2 - t_1)$ or

$$A_i = (2)^{-3/2} f_i(H_1 + H_2)(T_1 + T_2)^{\frac{1}{2}}(t_2 - t_1) \qquad (12)$$

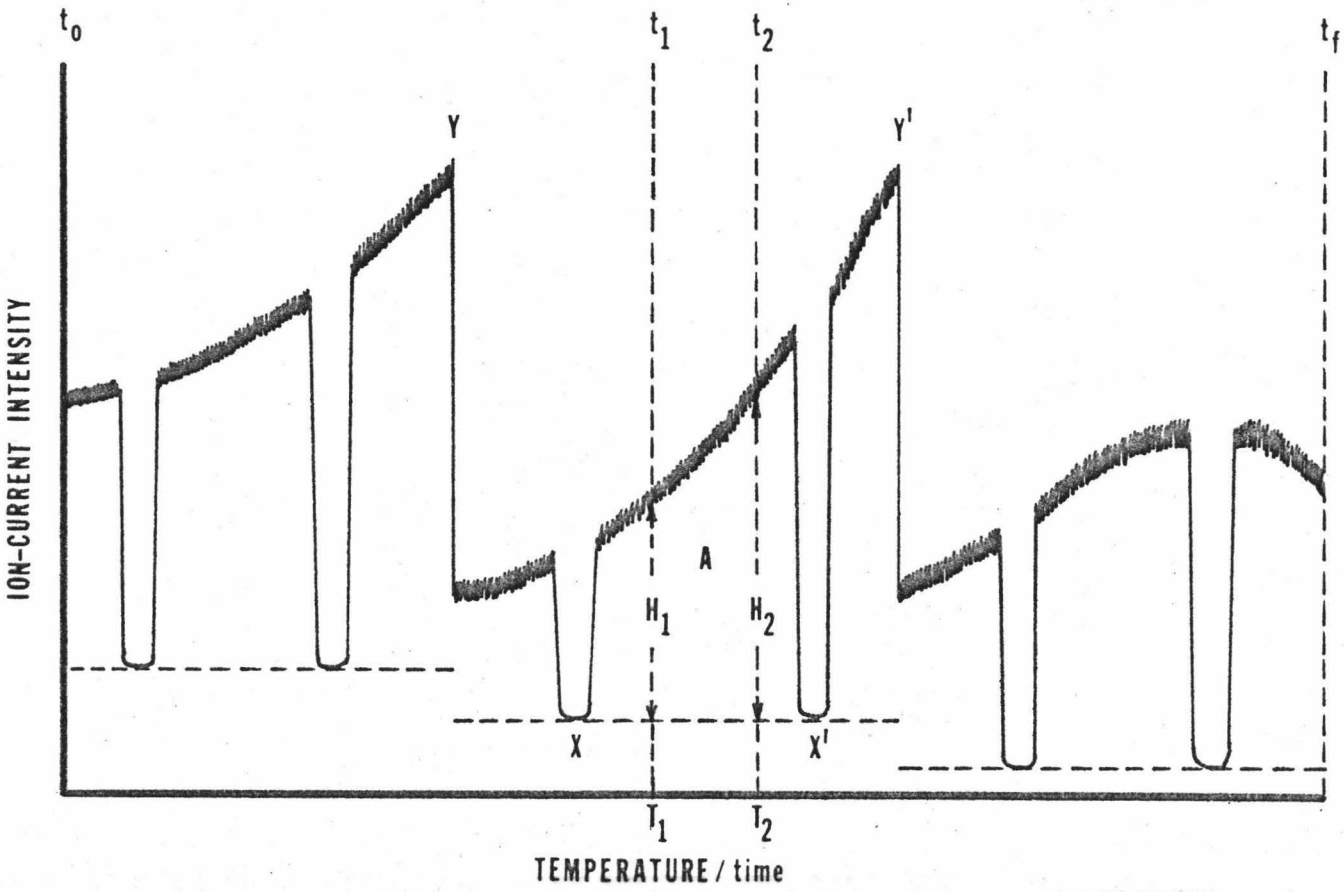

FIGURE 8 Illustration of the Graphical Integration Procedure for Quantitative Mass Spectrometric Analysis.

The analytical mass peak height was converted to the ion-current for specie i by the relationship

$$I_i^+ = \left(\frac{1}{C}\right)\left(\frac{1}{I_x}\right)\sum\left(\frac{H_i}{G\ T_q}\right) \qquad (13)$$

where C is the isotopic abundance characteristic of the analytical mass peak, I_x is the ionization efficiency, G is the electron multiplier gain (first dynode), and T_q is the quadrupole transmission efficiency. For the case of a monatomic analytical specie, it can be shown (see Appendix B) that Equations (11) and (13) imply $f_i = (C\ I_x\ G\ T_q)^{-1}$. Thus, Equation (12) becomes

$$A_i = (2)^{-3/2}(C\ I_x\ G\ T_q)^{-1}(H_1 + H_2)(T_1 + T_2)^{\frac{1}{2}}(t_2 - t_1) \qquad (14)$$

The total area under the strip chart trace was then the sum of the areas of the several trapezoidal sections, or, $A_{i,\text{total}} = \sum A_i$.

To eliminate the constant K_i from Equation (9) the mass spectrometer was calibrated by quantitatively vaporizing 2-6 mg portions of pure magnesium metal. The magnesium vaporized monatomically and gave isotopic mass peaks at m/e = 24, 25, and 26 but the 24 peak was monitored to obtain reference standard traces of the form depicted in Figure 8. Substitution of the results for the standard, s, into Equation (10) gives

$$W_{i,total} = W_{s,total}\left(\frac{M_s}{M_i}\right)^{\frac{1}{2}} \frac{\sum A_i}{\sum A_s} \qquad (15)$$

Equation (15) was used to calculate the mass of alkali which was vaporized during each quantitative mass spectral analysis. The values of C, I_x, G, and T_q which were used to compute the necessary values of A_i and A_s in Equations (14) and (15) are tabulated and discussed in Appendix B.

As a check on the accuracy of the determinations of W_{Na} and W_K, mass spectrometric measurements of alkali vaporization rates were made for samples of Hawaiian basalt HK-123 (Derby, 1970, page 70) and were compared with those obtained from samples of the same rock by Derby (1970) who used an independent vacuum deposition technique with analysis by atomic absorption spectrophotometry. The comparison of the two sets of results is shown in Table 3. The vacuum deposition rates at 1000° C were obtained by interpolation of rates at 990° C and 1010° C which were reported for 0.250 g samples by Derby (1970, page 91). The uncertainties quoted for the vacuum deposition data were derived from the cumulative uncertainties given by Derby (1970, pages 90-92) while the uncertainties given for the mass spectrometric data are the deviations observed for replicate analyses.

The data in Table 3 show acceptable agreement between the two independent techniques although the mass spectrometric values may be systematically higher. It will be

Table 3

A Comparison of Alkali Vaporization Rates
Determined by Knudsen Cell-Mass Spectrometry
And Vacuum Furnace Deposition,
Basalt Sample HK-123

Na Vaporization Rates ($\mu g \cdot g^{-1} \cdot hr^{-1}$) at 1000° C

Mass Spectrometry[a]	Vacuum Deposition[b]
176 ± 18	132 ± 29

K Vaporization Rates ($\mu g \cdot g^{-1} \cdot hr^{-1}$) at 1000° C

Mass Spectrometry[a]	Vacuum Deposition[b]
101 ± 10	73 ± 3

---

[a] determinations made in this study.

[b] rates derived from data in Table VIII, page 91, Derby (1970).

shown later, however, that the absolute accuracy of the vaporization rates was only of secondary importance to this investigation. The principal utility of the vaporization rates was the elucidation of the relative rates of alkali loss from the different sample materials.

3. Measurement of Alkali Vapor Pressures

The partial pressure, P_i, of a specie i is related to its mass spectrometric ion-current intensity as

$$P_i = k\, I_i^+\, T \qquad (16)$$

where T is the temperature (^oK) of the sample and k is an instrumental sensitivity factor (Grimley, 1967). In this investigation, the known vapor pressure of magnesium metal as a function of temperature (Nesmeyanov, 1963) was used to evaluate k in Equation (16). The vaporization behavior and analytical parameters (see Appendix C) of magnesium metal should be sufficiently similar to those for sodium and potassium to make the calibration valid for the alkalis. Extension of the magnesium calibration data to the calculation of partial pressures of the permanent gases (CO_2, N_2, etc.) is probably more tenuous and, therefore, was not attempted.

The calibration data is summarized in Figure 9 which shows a plot of log P_{Mg} vs 1/T constructed from the magnesium vapor pressure data of Nesmeyanov (1963).

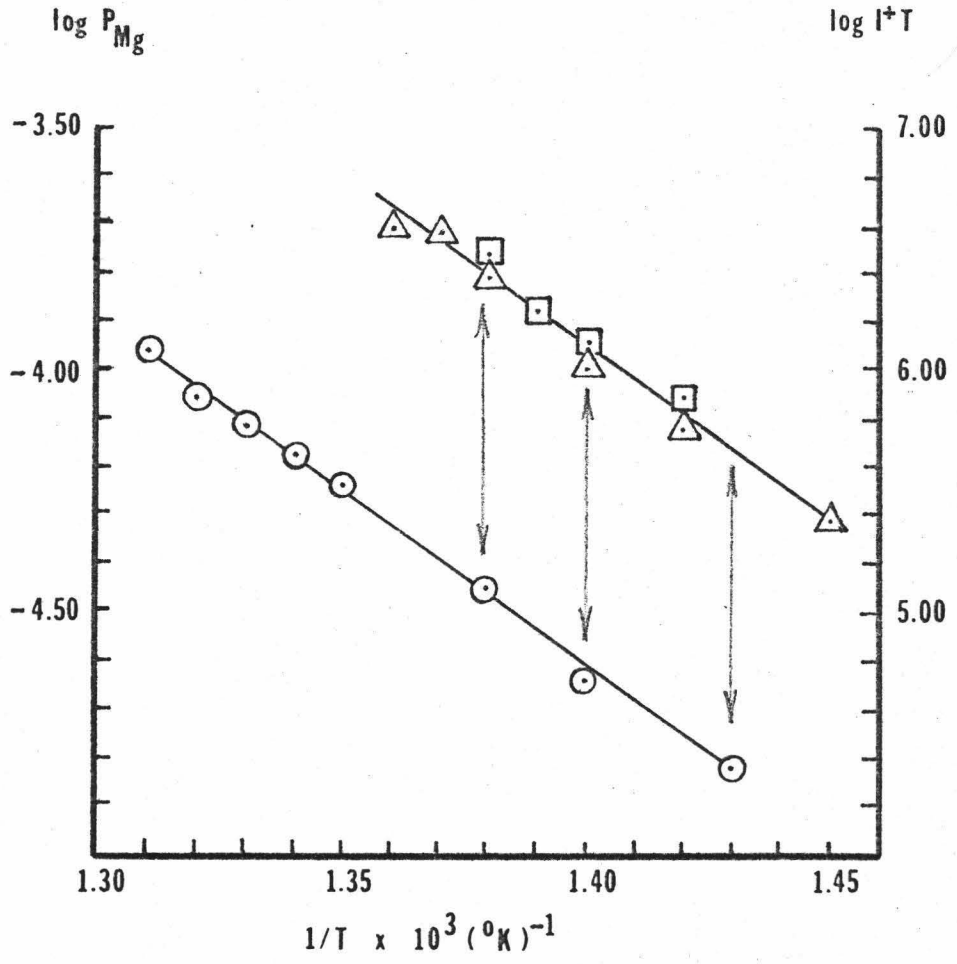

FIGURE 9 Calibration Plot for Mass Spectrometer Sensitivity Determination. The arrows indicate the data points selected for evaluation of the sensitivity constant (see text for explanation).

A similar plot of log I_i^+T vs. 1/T was constructed from measurements made during the vaporization of magnesium metal in the Knudsen cell-mass spectrometer system. As would be expected from the terms of the Clausius-Clapeyron equation and Equation (16) both sets of data points in Figure 9 give linear plots. The lines drawn through the respective sets of data points are visual best fits and are approximately parallel as should also be the case since the slopes of both lines represent $\Delta H_{vap}/2.303R$ where ΔH_{vap} is the enthalpy of vaporization of magnesium and R is the gas constant.

Equation (16) can be rearranged in logarithmic form as

$$\log k = \log P_i - \log I_i^+T \qquad (17)$$

To evaluate the sensitivity constant, k, three sets of corresponding points on the two calibration plots were selected as shown in Figure 9. The mean of the three results as computed from Equation (17) was taken as the value of k.

It should be noted that two sets of mass spectrometric calibration data were used in constructing the log I_i^+T vs. 1/T plot in Figure 9. The first set (open triangles) was collected near the beginning of the pressure measurement phase of the project while the second set (open squares) was collected seven months later, near the end of the project. The two sets of data are in good agreement, indicating that the mass spectrometer sensitivity was essentially constant during the course of this investigation.

The corrected values of I_i^+ were expressed in millivolts such that the value obtained for the sensitivity constant was $k = 2.2_4 \times 10^{-11}$ atm $(mv)^{-1}(^oK)^{-1}$. The vapor pressures of Na and K observed for the vaporized rock samples were computed by the appropriate substitution of k into Equation (16).

III. RESULTS AND DISCUSSION

A. Results of Vaporization Experiments

1. General Observations

The general vaporization behaviors of the various rock materials were determined by mass spectrometric scanning surveys as previously described (see pages 24-26). The four different types of sample materials which were studied (see Table 2, page 8) consisted of Hawaiian tholeiitic basalts (B1-B4), plagioclase feldspar (P), Australasian tektites (T1, T2), and the Allende carbonaceous chondrite (M). The vaporization behaviors of the four groups are summarized in the mass pyrograms of Figures 10 and 12-14 which have been plotted on the same scale to facilitate comparison.

The four basalts showed virtually the same gas-release patterns as exemplified in the mass pyrogram of Figure 10. Water was the most abundant volatile compound released and appeared to emanate from both low temperature (200-400° C) and high temperature (500-975° C) sources. The peaks at 700° C and 850° C in the high temperature portion of the H_2O release curve did not appear in the mass pyrograms of all basalt specimens. However, all basalt samples did consistently demonstrate maximum H_2O release at points inside the 700-850° C range. The low temperature and high temperature episodes of H_2O release probably represent surface desorption and chemical exsolution processes,

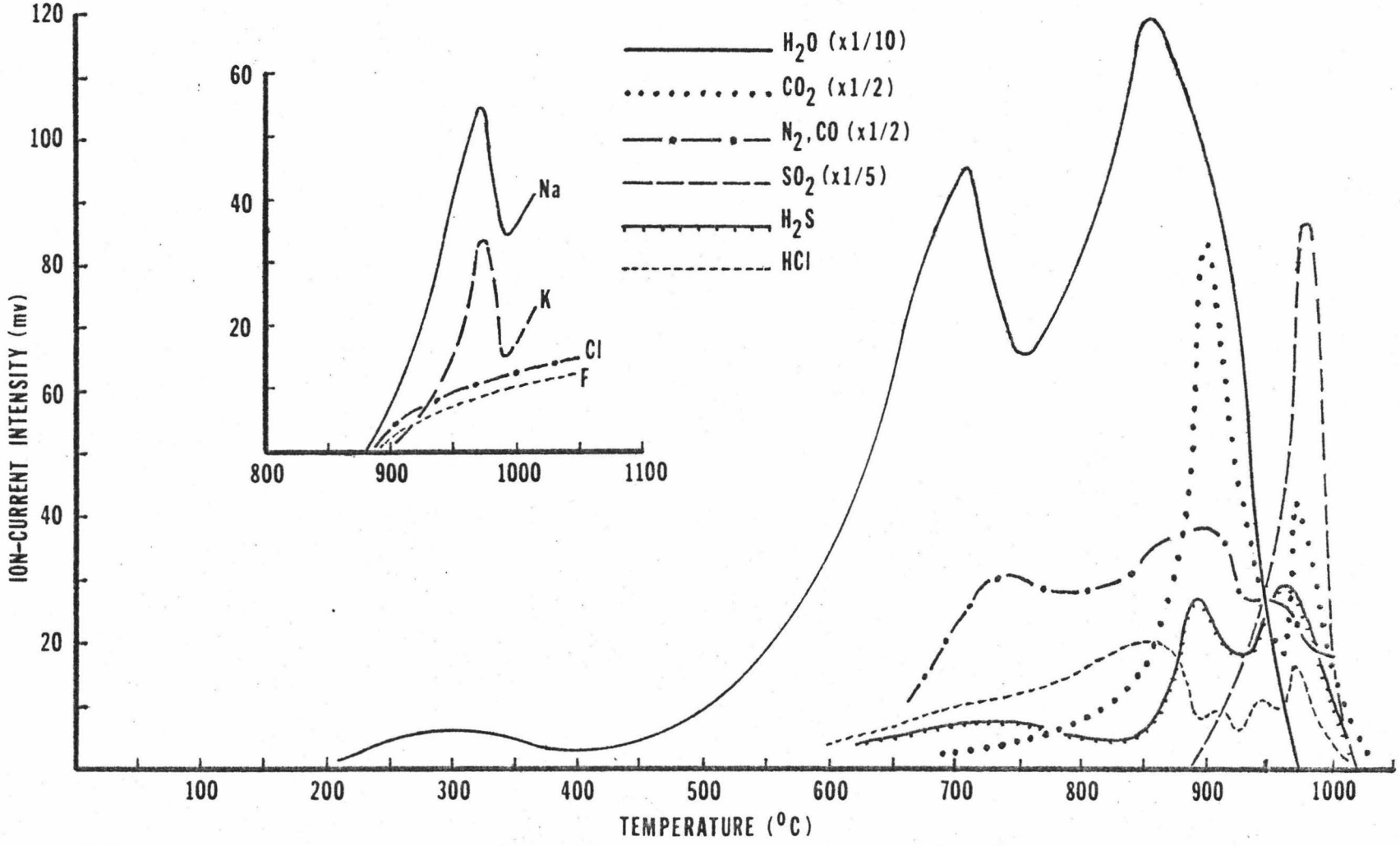

FIGURE 10 Mass Pyrogram for Basalt B2.

respectively. In addition to H_2O, carbon and sulfur gases were prominent members of the volatile phase which was released from the basalts. As is usually the case in low-resolution mass spectrometry, the distinction between CO and N_2 was difficult since both species give parent ion peaks at m/e = 28. However, high-resolution mass spectrometric studies of Hawaiian basalts by Simoneit, et al. (1973) suggest that the ion-current from m/e = 28 is, at high temperatures, almost certainly due to CO^+. Inert gases (He, Ar, etc.) were probably also released in small amounts from the basalts but were not studied because of their erratic background signals which resulted from intermittant backstreaming of inert gases from the ion pump in the mass spectrometer vacuum system.

Softening of the basalt specimens began at about 900° C followed by the appearance of SO_2 and additional CO_2 as melting and vesciculation proceeded. Vigorous bubbling of the molten samples continued until degassing was completed. During melting and vesiculation the basalts became highly mobile and tended to creep up the sides of their Lucalox® containers (see page 21), sometimes blocking the molecular beam orifice. Thus, complete degassing of the samples (by heating at 1000-1020° C for about 30 min) was necessary before higher temperatures could safely be achieved. Proper selection of sample size and operating procedure ordinarily reduced the sample creep problem to a tolerable level.

Although Figure 10 is a gas-release profile for one of the submarine basalts, B2, the same species were also observed in lesser abundances from the subaerial basalts, B3-B4.

The vesiculation of the basalts over the 900-1000° C range produced scoriaceous residues as shown in Figure 11. Heating of the degassed residues to about 1100° C transformed them into glasses with generally smooth surfaces and few vesicles.

The vesiculation of the initial gas-rich basalts was observed mass spectrometrically in the form of ion-current surges at certain mass numbers and, occasionally, as pressure surges on the ionization gauge. Ion-current surges were typically observed at mass numbers 28 (N_2^+, CO^+), 44 (CO_2^+), 48 (SO^+), and 64 (SO_2^+). Assuming that the fragment ions CO^+ and SO^+ were responsible for the surges at mass numbers 28 and 48, respectively, it was concluded that CO_2 and SO_2 were the gases primarily responsible for the vesiculation of the basalts over the 900-1000° C range during the vacuum fusion experiments. Ion-current surges at mass number 18 (H_2O^+) were usually observed over the 700-850° C range but were rarely observed over the 900-1000° C range. Occasionally, ion-current surges were also observed over the 900-1000° C range at mass numbers 23 (Na^+) and 39 (K^+).

The tektite specimens, T1 and T2, showed very little gas release. A mass pyrogram for T2 is shown in Figure 12 and is nearly identical to that observed for T1.

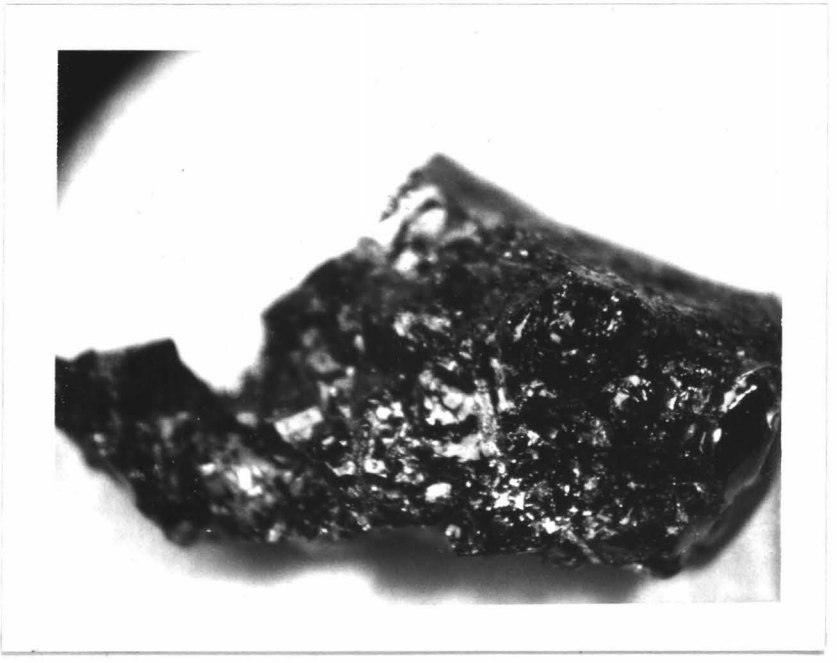

(a)

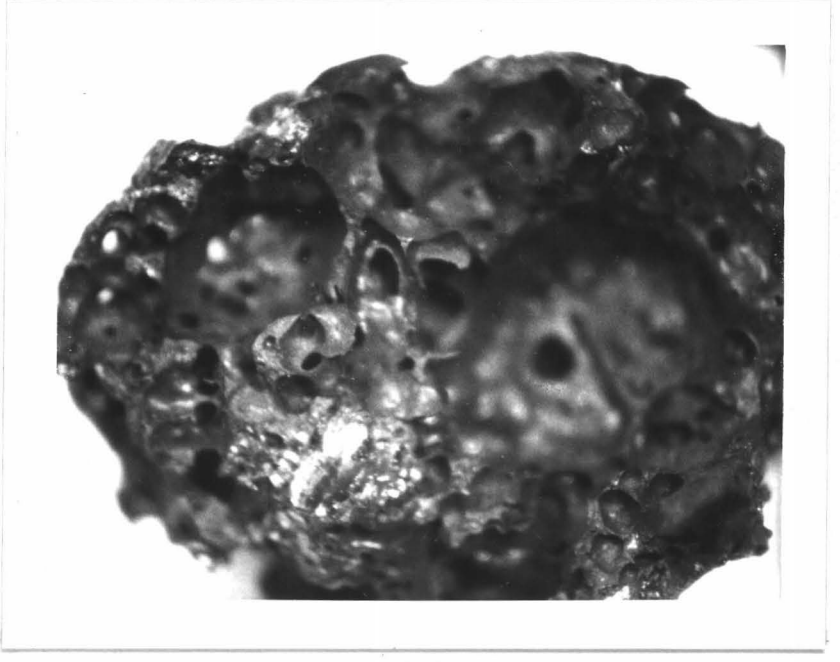

(b)

FIGURE 11 Specimens of Basalt B1 (a) Before and (b) After Fusion at 1000° C in a Vacuum of 10^{-7} Torr. Both photographs represent 20X magnification.

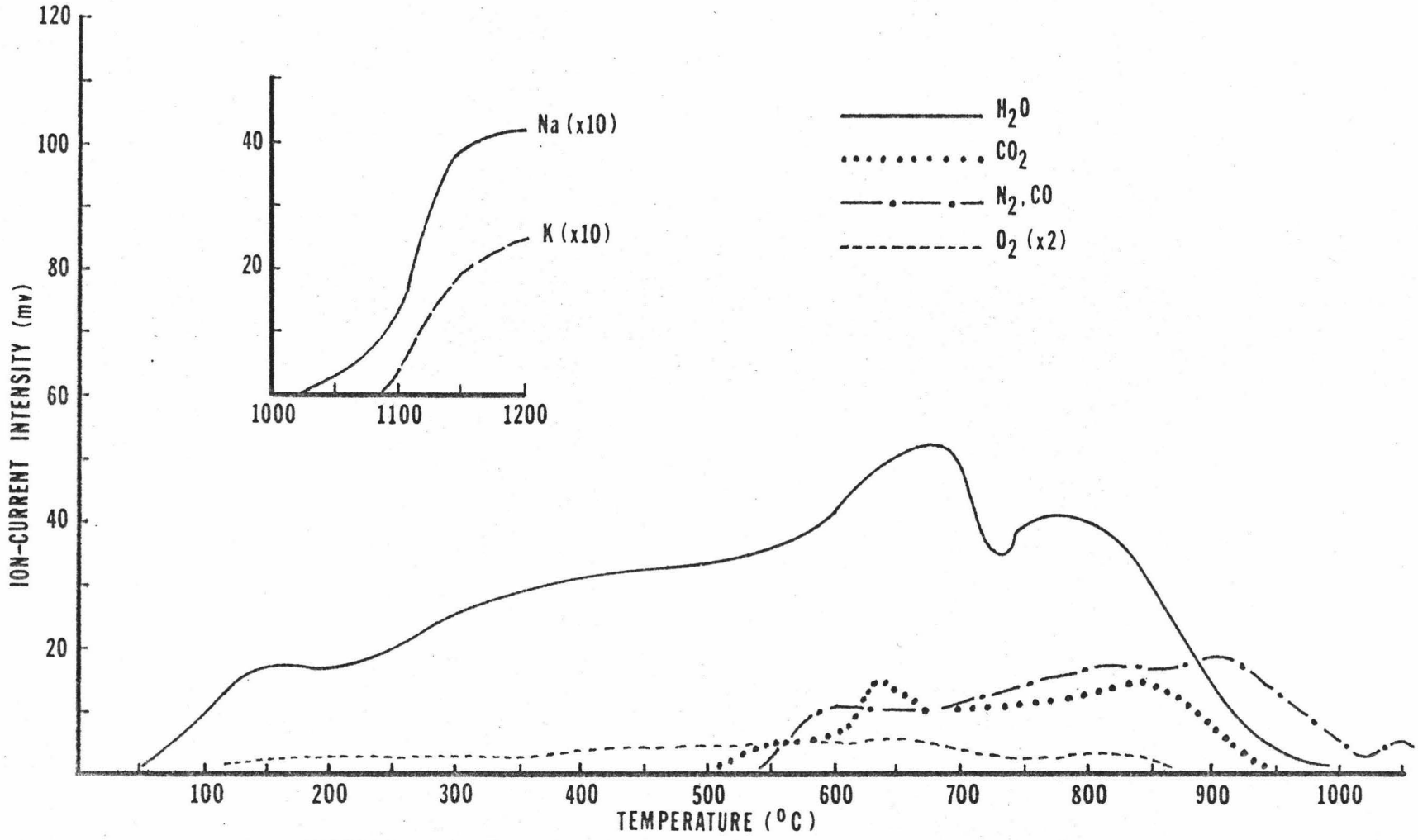

FIGURE 12 Mass Pyrogram for Tektite T2.

Comparison of Figures 10 and 12 , which are plotted on the same scale, demonstrates the great difference in volatile contents between the basalts and tektites. The small amounts of gas which were released from the tektites were similar in composition to those reported for other tektite specimens by Friedman (1963). The tektites partially melted inside the 900-1000° C range but because of their higher viscosities and lower gas contents did not vesiculate and flow as extensively as did the basalts.

Sample P, the plagioclase feldspar, released very little gas during vacuum heat treatment as can be seen in Figure 13. Furthermore, little if any gas release was apparent at temperatures above 900° C where the vaporization of the alkalis began.

Sample M, the Allende carbonaceous chondrite, showed both a large release of gases and alkali vapors as is evident in Figure 14. The total volume of gas released from the meteorite was several times greater than that from the basalts and the compositions of the respective gas phases were significantly different. Carbon and sulfur gases were major constituents in the gas phases of both sample materials although the meteorite gas phase showed a generally lower oxidation state than that of the basalt gas phase. The gases CO and S_2 were prominent among the species released from the meteorite while CO_2 and SO_2 were more abundant in the gas phase derived from the basalts. The difference in oxidation states of the respective gas

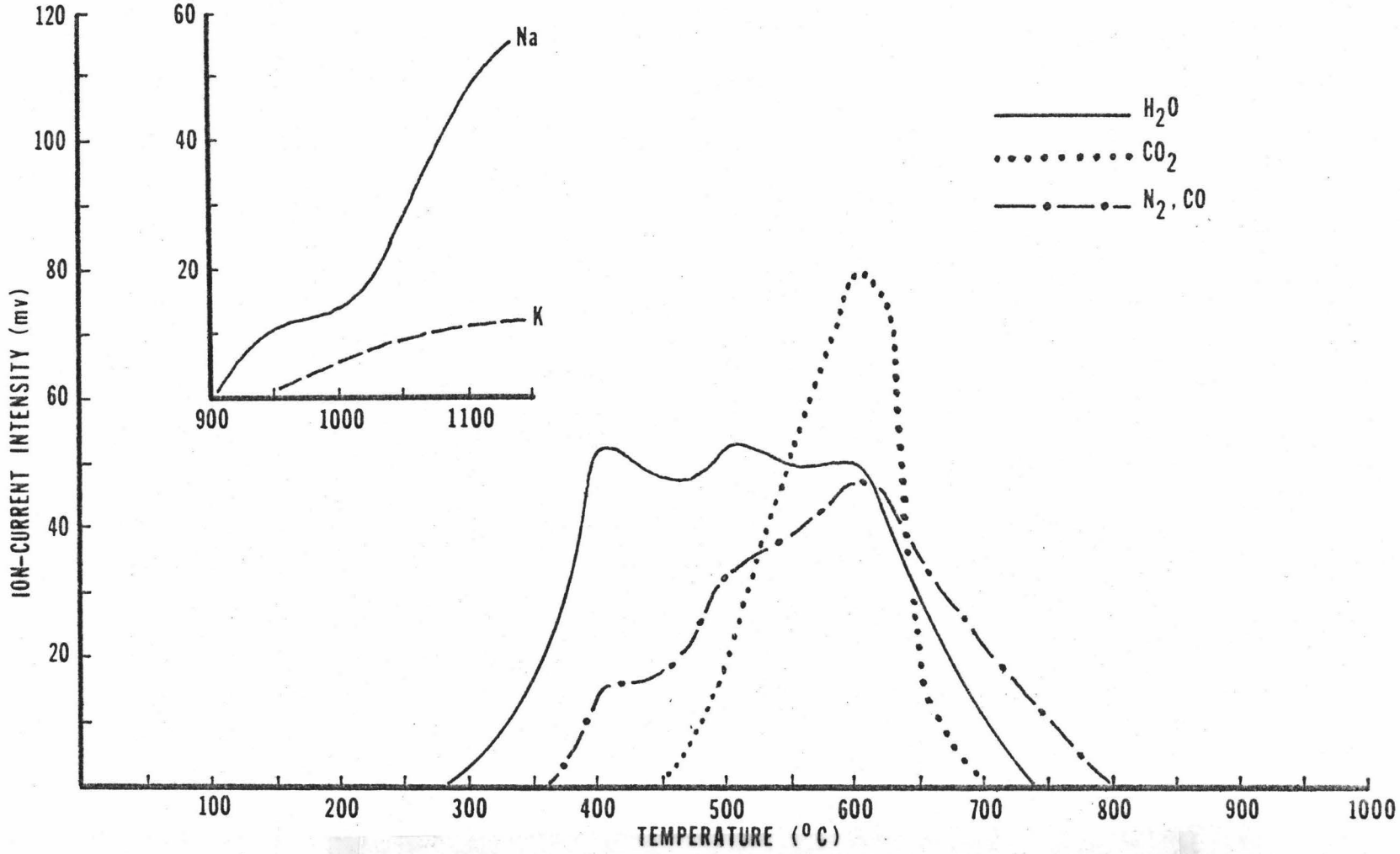

FIGURE 13 Mass Pyrogram for Plagioclase Feldspar P.

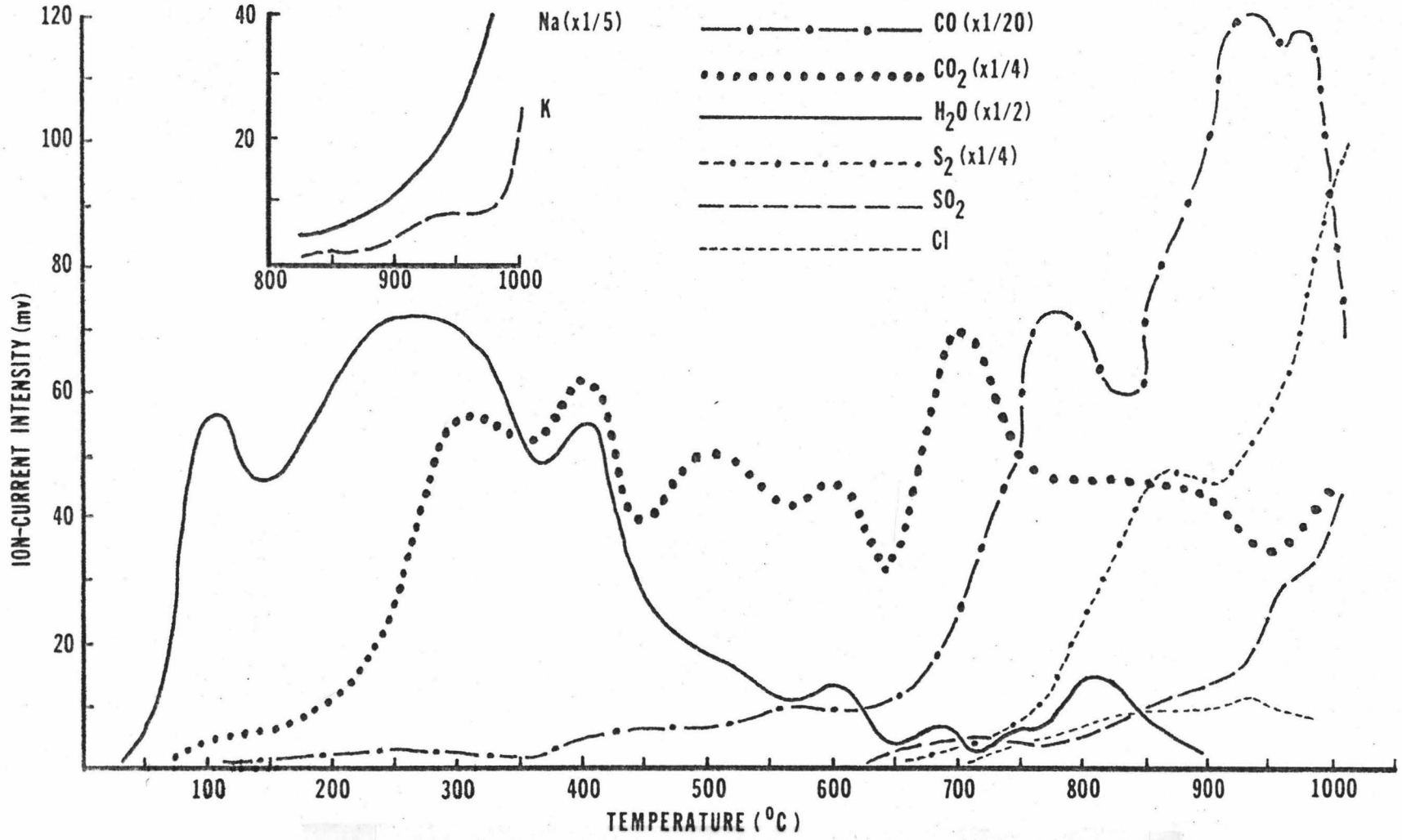

FIGURE 14 Mass Pyrogram for Allende Carbonaceous Chondrite M.

phases is consistent with the difference in oxidation states of iron in the two sample materials. The meteoritic iron exists as Fe° and Fe(II) while the basaltic iron occurs as Fe(II) and Fe(III) (See Table 1, page 2). In further contrast, less H_2O was released from the meteorite than from the basalts. The release of H_2O from the meteorite occurred mostly at low temperatures (100-600° C) whereas the majority of the basaltic H_2O was released at high temperature (700-975° C).

The four types of materials which were studied can be roughly divided into two groups on the basis of their vaporization behaviors. The first group, consisting of the basalts and the Allende carbonaceous chondrite, can be called "gas-rich" because of their release of large amounts of gases during heat treatment. The second group, consisting of the plagioclase feldspar and the tektites, can be called "gas-poor" since they released comparatively small amounts of gas upon heating. A careful comparison of Figures 10 and 12-14 also reveals that the gas-rich group of materials demonstrated a higher rate of alkali vaporization than did the gas-poor group. The possible relationship between gas release and alkali vaporization will be examined in the next section.

2. Bimodal Alkali Release from Basalts

In addition to the general differences in vaporization behavior between the basalts and other sample materials the

basalts exhibited a peculiar type of alkali vaporization. As shown in Figure 10, alkali vaporization from the basalts began at approximately 900° C and showed a maximum at about 975° C, followed by a smooth and continuous increase above 1000° C.

The maxima in the alkali release curves can be interpreted in a number of ways. First, the vascillatory vaporization profiles could represent instrumental fluctuations which resulted in the registration of erroneous ion-current signals. However, the data to be presented shortly should demonstrate convincingly that the reproducibility of the effect was great enough to confidently discount instrumental errors as the basis of the effect. A second possibility is that the alkali vaporization curves represent the superposition of vaporization contributions from two separate sources. Because the mass spectral background ion-current intensities were carefully monitored throughout this study it can be stated with confidence that the effect was not due to background sources of alkalis in the analytical system. Assuming the bimodal effect to be real, the two sources of alkalis might be contained in the samples themselves. Two of the basalts used in this investigation were formed in submarine eruptions so that sea water contamination might immediately be suspected. Contrary to that expectation, Moore (1965) and Hart (1973) found no evidence that significant sea water contamination of the samples had occurred. Exchange of inert gases between sea-water and freshly erupted submarine

basaltic lava probably occurs (Fisher, 1971) but exchange of major elements and nongaseous trace elements is thought to be minimal (Hart, 1973). Furthermore, the bimodal form of alkali release was observed not only from the submarine basalts but also from the subaerially erupted basalts. As mentioned previously, the subaerial basalts were collected very soon after eruption (see Table 2, page 8) and should be as free of contamination as can reasonably be expected. Thus, the bimodal form of alkali vaporization from the basalts must represent some effect which is characteristic of the samples but which is not related to contamination.

Early in this investigation it was noticed that the maxima in the alkali vaporization profiles for the basalts seemed to coincide with maxima in the release profiles of SO_2 and CO_2 over the 900-1000° C range (see Figure 10, page 39). The maxima of the respective ion-current intensity curves apparently were related to the episodes of most vigorous degassing of the basalts, usually between 950° C and 1000° C. The reproducibility of the effect led to a search for some relationship between vesiculation processes and the episodes of accentuated alkali vaporization. The results of those studies will now be presented and discussed.

The 900-1000° C range was chosen for quantitative study of alkali vaporization since it was the range in which vesiculative degassing of the basalts occurred. The alkali loss rates were determined for all samples by the procedure

described previously (see pages 26-32) and are summarized in Figures 15 and 16. Both figures exhibit three general features: (1) for all samples, the alkali loss rates are greater during degassing (Type I vaporization) than during reheating of the degassed residues (Type II vaporization), (2) for individual samples, the alkali loss rates are more variable during Type I vaporization than during Type II vaporization, and (3) there is no clear relationship between the Type I vaporization rates and the initial alkali concentrations although a concentration-Type II vaporization correlation might exist.

Because the initial alkali concentrations in the samples should govern, at least in part, the rates of alkali vaporization the results in Figures 15 and 16 have been arranged according to increasing Na_2O and K_2O concentrations in order to emphasize that a concentrational control of vaporization does not adequately explain the observations.* The tektites possessed five times more K than the basalts but demonstrated K vaporization rates which were 10-50 times smaller than those of the basalts. A comparable inconsistency exists between the tektite and basalt rates of Na vaporization. Similarly, the plagioclase feldspar (P) possessed more Na than the basalts but vaporized it at a much lower rate. The Allende meteorite (M) possessed very low

---

* The Na and K concentrations in the initial samples were determined by Virginia A. Lewis using atomic absorption spectrophotometry. The results were converted to percent Na_2O and K_2O to match petrological convention.

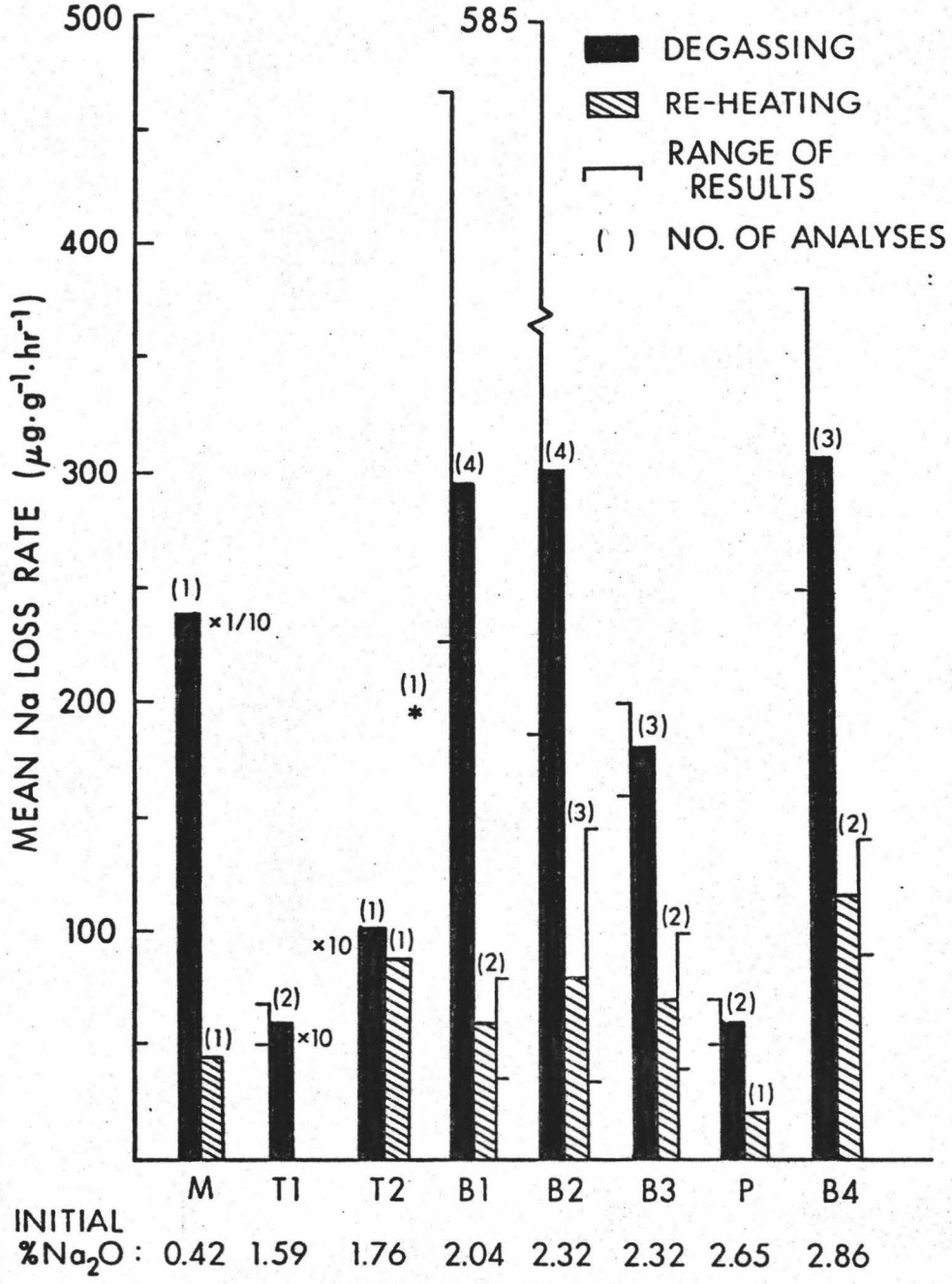

FIGURE 15 Mean Sodium Vaporization Rates Over the 900-1000° C Range.

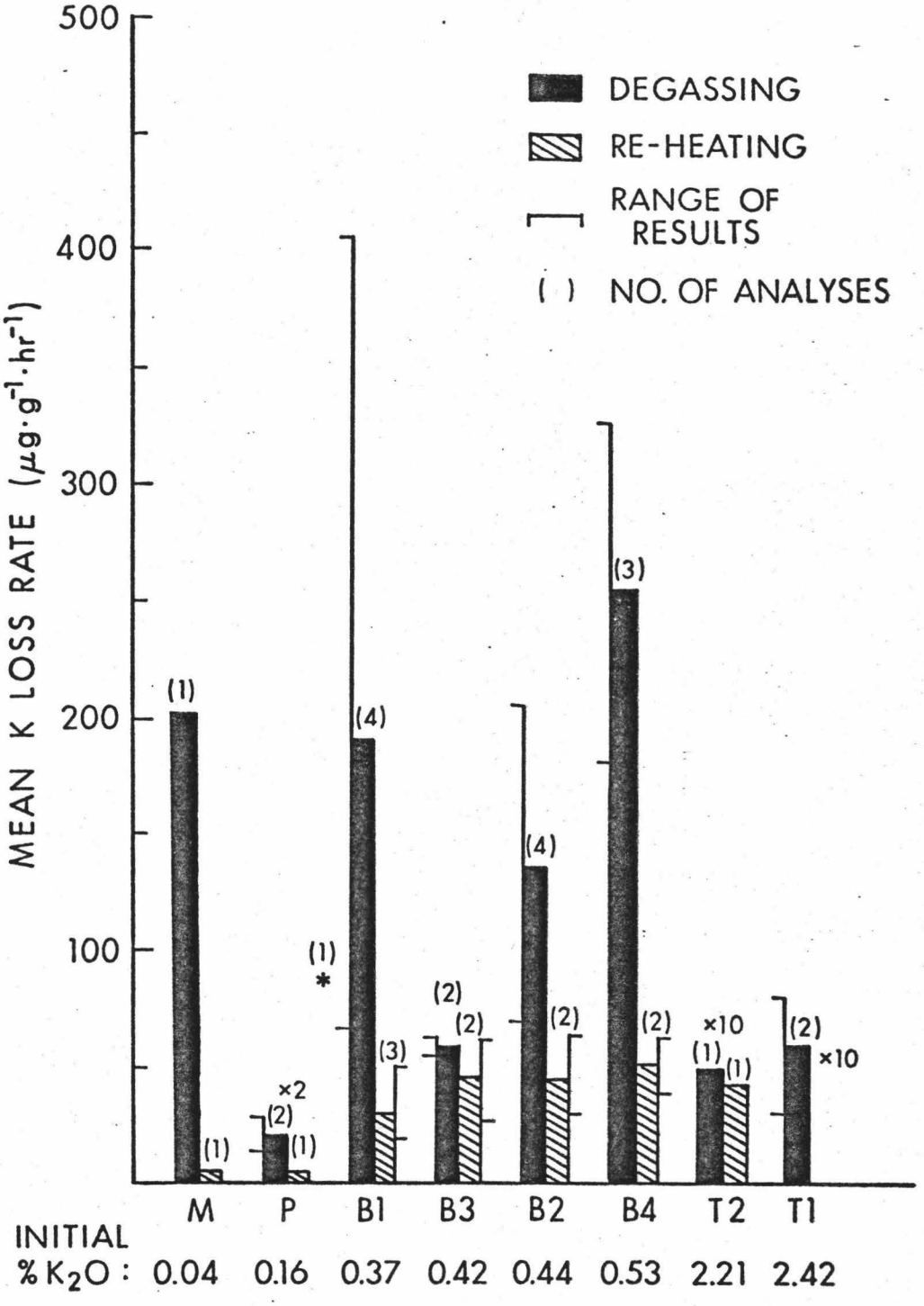

FIGURE 16 Mean Potassium Vaporization Rates Over the 900-1000° C Range.

alkali concentrations yet exhibited surprisingly high rates of alkali vaporization. Clearly, the rates of Type I alkali vaporization from the samples were not controlled by initial alkali concentration.

Type II alkali vaporization (i.e. vaporization of previously degassed sample residues) showed somewhat more predictable rates which might be controlled principally by initial alkali concentrations although the tektites still present an inconsistency.

Thus, other factors such as viscosity must be considered in explaining the vaporization results. In that regard, it should be noted that over the 900-1000° C range sample P remained solid, M melted only slightly, T1 and T2 were partially melted, while B1-B4 were totally melted (excepting phenocrysts). The range of viscosities was obviously wide but among the sample materials which were studied the basalts and tektites were most nearly comparable in terms of their initial alkali concentrations and fluidities at 1000° C. Still, the rates of alkali vaporization were 50-60 times greater from the basalts than from the tektites (see Figures 15 and 16). Only at about 1200° C did the tektite vaporization rates begin to approach those of the basalts at 1000° C.

Comparing B1-B4 with P, it is clear that the presence of plagioclase phenocrysts in the basalts does not explain the tektite/basalt vaporization rate discrepancy. Even if the plagioclase in the basalts did react with the melt to release more alkalis the tektite/basalt alkali concentration

ratios would not differ from the alternative case in which the plagioclase did not react. In fact, the partitioning of some of the basaltic alkalis into more restrictive solid crystals such as plagioclase should decrease their overall rates of loss by vaporization. However, the experimental observations are to the contrary since the basalts showed greater Na vaporization rates than did the plagioclase even though the latter material possessed a greater initial Na concentration.

From a thermodynamic standpoint, the vaporization of alkalis should be favored by large sample surface areas for a given set of initial concentrations. In that respect the basalts differ from the other sample materials in that their bulk volumes were composed of 1-75% vesicles (see Table 2, page 8). However, it was observed that the vesiculative degassing of the basalts consistently produced scoriaceous residues which were clearly more vesicular than the initial specimens (see Figure 11, page 42). In contrast the tektites fused into spheroidal globules. Thus, first melting of the basalts markedly increased their specific surface areas such that alkali vaporization should have been even more favorable during subsequent heating runs since it can be shown that their alkali concentrations did not decrease significantly during the first vacuum fusion step.

Assuming alkali loss rates of 300 μg Na/g/hr (see Figure 15) and 140 μg K/g/hr (see Figure 16) for basalt B2, a 1 g sample should lose only 300 μg of it initial

17,200 μg Na [=(1 g)(0.0232 g Na_2O/g)(46 Na/62 Na_2O) 10^6 μg/g)] and only 140 μg of its initial 3650 μg K [=(1)(0.0044)(78.2/94.2)(10^6)] during 1 hr inside the 900-1000° C range. Such losses would reflect relative alkali depletions of only 1.7% initial Na_2O and 3.8% initial K_2O. The predictions are supported by the results of atomic absorption analyses of some of the post-fusion scoriaceous residues as shown in Table 4. Oddly enough, the alkali concentrations seemed to increase during vacuum vaporization in all cases except that of B3. Allowing for analytical uncertainties, though, no systematic trend in the alkali concentrations can be claimed. For example, the analytical uncertainties for sample B4 include the possibilities that the initial alkali concentrations were 2.20% Na (= 2.12 + 0.08) and 0.42% K (= 0.44 - 0.02) while the concentrations in the post-fusion residue were 2.22% Na (= 2.31 - 0.09) and 0.40% K (= 0.38 + 0.02). The implication would then be that vaporization increased the Na concentration while it decreased the K concentration. A similar appraisal of B3 would lead to opposite conclusions. Regardless of whether the apparent concentrational increases of Table 4 are real or are analytical artifacts, it can be concluded that the effect of interest, namely alkali concentration decreases due to vaporization, did not occur to a substantial degree.

Thus, both the alkali vaporization rates measured mass spectrometrically and those measurements attempted by atomic

Table 4

Alkali Concentrations[a] in Basalt Samples
Before and After Vacuum Fusion

Sample	% Na before	% Na after[b]
B1	1.51 ± 0.06	1.85 ± 0.07
B3	1.74 ± 0.07	1.83 ± 0.07
B4	2.12 ± 0.08	2.31 ± 0.09

Sample	% K before	% K after[b]
B1	0.33 ± 0.01	0.37 ± 0.01
B3	0.35 ± 0.01	0.33 ± 0.01
B4	0.44 ± 0.02	0.38 ± 0.02

---

[a] determinations made by Virginia A. Lewis using atomic absorption spectrophotometry. A relative error of 4% was assumed for all results.

[b] data for aliquots of approximately 200 mg after heating for 1 hr at 1000° C in a vacuum of 1 x 10^{-7} torr.

absorption spectrophotometry indicate that the alkali concentrations in the basalt samples should be essentially the same at the start of both the first and second fusion runs. However, the specific surface areas of the specimens should definitely be greater at the start of the second fusion runs so that alkali vaporization should theoretically be more favorable during second fusion runs. That is, Type II vaporization rates should be greater than Type I vaporization rates according to thermodynamic reasoning. Clearly, the data in Figures 15 and 16 contradict that expectation, leading to the conclusion that factors other than specific surface area of the starting material must influence the alkali vaporization rates of the basalts.

There remains a final important difference between the basalts and the other samples investigated, namely their initial contents of gas-forming volatiles. As originally stated, one of the principal aims of this research was to observe the vesiculation of basalts under high vacuum. That objective was accomplished by the use of gas-rich, glassy rocks B1-B4. Having failed to explain the observed rates of alkali vaporization by other criteria, one might postulate that the high rates which occur upon first fusion of the basalts are the results of effects inherent in the vigorous degassing of the samples.

To test the hypothesis of accelerated vaporization by vesiculation, studies were conducted on the vaporization behavior of portions of B1 which had been crushed to 115

mesh ASTM (0.125 mm). Presumably, the increased specific surface area of the crushed sample should favor the increased vaporization of alkalis while the release of trapped gases by crushing would reduce the rate of alkali vaporization if the vesiculation hypothesis was correct. The results for the crushed samples (indicated with a * in Figure 15, page 51, and Figure 16, page 52) were found to fall clearly below the average for the whole rock (5-10 mm) specimens. Like the whole-rock specimens, the crushed rock ultimately fused and vesiculated although the total amount of gas released in the process was noticeably less than that observed from the whole-rock specimens. The difference can be attributed to the removal of a larger portion of the total gas content of the crushed rock at subsolidus temperatures.

The volumetrically lower gas release from the B1 crushed rock may bear on the wide range of results observed during Type I vaporization studies of the whole-rock basalts. Given the apparent influence of gas release on alkali vaporization rates, an inhomogeneous distribution of occluded or dissolved gases in the original samples could widen the range of observed vaporization rates when small chunks of variable size are employed as specimens. The generally lower ranges observed for Type II vaporization runs on the same samples are consistent with such an explanation.

The compositions of the gas phases observed during the fusion and vesiculation of the basalts are summarized in

Table 5. Sample M, even though it did not vesiculate over the 900-1000° C range, did release large amounts of gas and is therefore included for comparison. The lesser amounts of gas released from samples P, T1, and T2 occurred principally at temperatures below 900° C (see Figure 12, page 43, and Figure 13, page 45) so that gas phase compositions for those samples are not included in Table 5. The vapor phases of samples M and B1-B4 were, of course, rich in Na and K but the results in Table 5 were calculated on an alkali-free basis.

As explained previously, the gases were identified by their ion-fragmentation patterns, isotopic patterns, and shutterabilities. The much greater shutterability of S_2 allowed its distinction from SO_2 even though both species gave parent peaks at m/e = 64 in sample M. The difficulty in distinguishing N_2 from CO has been discussed (see page 40) but it is likely that, at m/e = 28, most of the ion-current at low temperatures was from N_2^+ while most on the ion-current at high temperatures was from CO^+ (Simoneit, et al., 1973). For sample M, though, the fragmentation pattern (Including large m/e = 12 (C^+) peak) was definitive for CO. Fluorine, as F^+ (m/e = 19), was observed from all four basalt samples but its variability above background led to the assumption that %F = %Cl in the gase phase, in conformity with the similar concentrations of the two in the initial rock samples (see column 1, Table 1, page 2, and Moore, 1965).

Table 5

Mole Per Cent Composition of Basaltic and Meteoritic Gas Phases at 950° C

Gas	Sample No.								
	M	B1	B1	B2	B2	B3	B3	B4	B4
SO_2	2.3	46.9	40.8	55.2	63.9	18.9	14.1	62.5	26.8
S_2	9.5	-	-	-	-	-	-	-	-
H_2S	0.4	4.0	4.3	2.1	3.7	8.0	21.6	2.5	1.4
CO_2	7.4	17.7	18.0	22.5	16.0	5.7	4.8	-	13.1
CO, N_2*	76.9	11.5	11.4	7.6	7.2	24.1	-	-	26.1
H_2O	3.1	14.2	15.6	9.7	4.5	36.2	45.2	12.9	23.1
HCl	-	1.8	2.4	1.3	1.5	4.9	5.0	2.1	3.0
Cl	0.4	1.8	3.8	0.8	1.5	0.9	4.3	9.2	3.3
F*	-	1.8	3.8	0.8	1.5	0.9	4.3	9.2	3.3

Normalized total gas release (900-1000°C)*:	M	B1	B2	B3	B4
	23	2.3	3.6	1.3	1

†Compositions are calculated on an alkali-free basis at 950°C for a single analysis of M and duplicate analyses of B1-B4.

-Indicates no or negligible amount detected.

*See text for explanation.

By summing the ion-currents (which are proportional to partial pressures) of the non-alkali species at 950° C a further estimate was made of the relative volumes of gas which were released from the different samples over the 900-1000° C range. That data, normalized with respect to B4, is also given in Table 5 where, again, the gas-poor samples P, T1, and T2 have been excluded from the estimates.

While H_2O was the most abundant volatile in the total gas contents of the basalts, the data in Table 5 show that it did not dominate the gas phase which appeared during vesiculation. Carbon and sulfur gases were of equal or greater abundance than H_2O during vesiculation of the basalts. The vesiculative gases from the subaerially erupted samples (B3, B4) showed greater compositional variations than did those from the submarine samples (B1, B2), probably as the result of the more variable degassing histories of the former materials.

The experimental vapor pressure measurements (see pages 34-37) are summarized in Figures 17-21. In those diagrams, Clausius-Clapeyron plots have been constructed for each type of sample studied to facilitate comparison with similar data for lunar basalts 12022 and 12065 as reported by De Maria, et al. (1971). The most conspicuous features of the log P vs. 1/T plots are their linearity in all cases except those of the gas-rich basalts as represented by B2 (see Figures 17 and 18). Reheating of the degassed basalts (dashed lines in Figures 17 and 18) gave linear plots while the initial

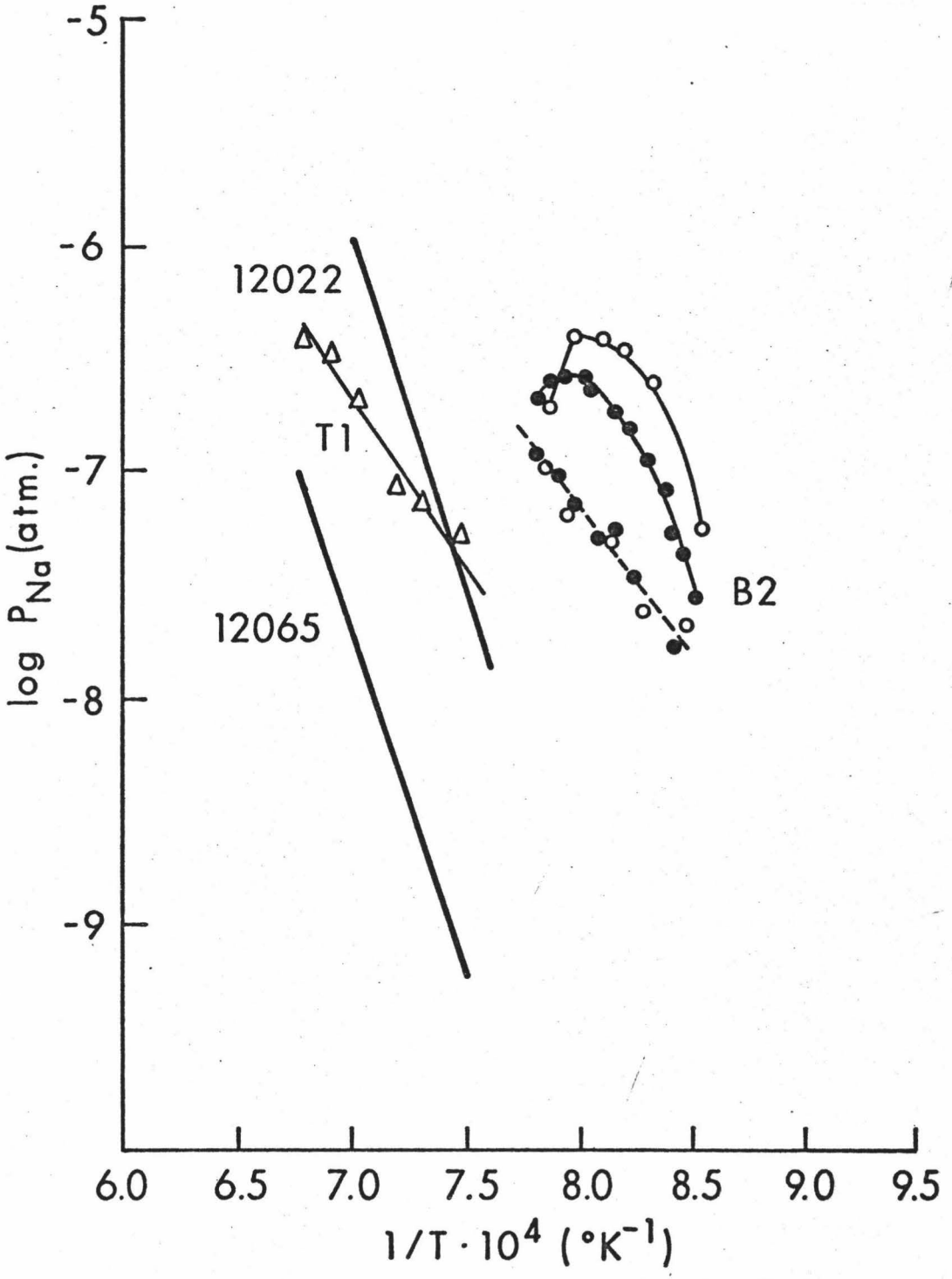

FIGURE 17 Sodium Vapor Pressure Comparison of Basalt B2 and Tektite T1 With Lunar Basalts 12022 and 12065. Solid B2 and T1 lines represent degassing; dashed line is reheating of degassed residue. Duplicate results are shown for B2 (solid and open circles, respectively).

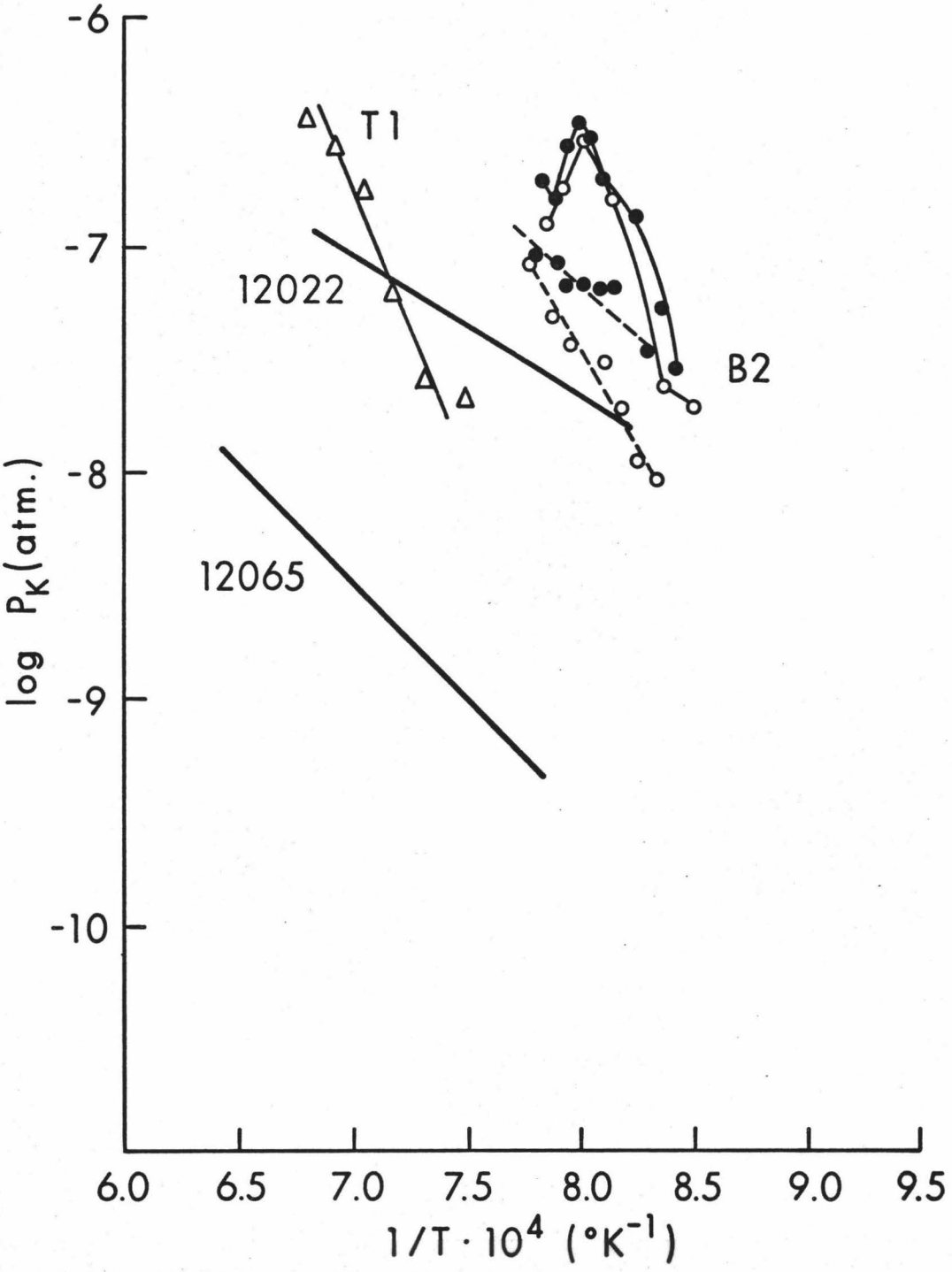

FIGURE 18 Potassium Vapor Pressure Comparison of Basalt B2 and Tektite T1 With Lunar Basalts 12022 and 12065. Additional description same as for Figure 17.

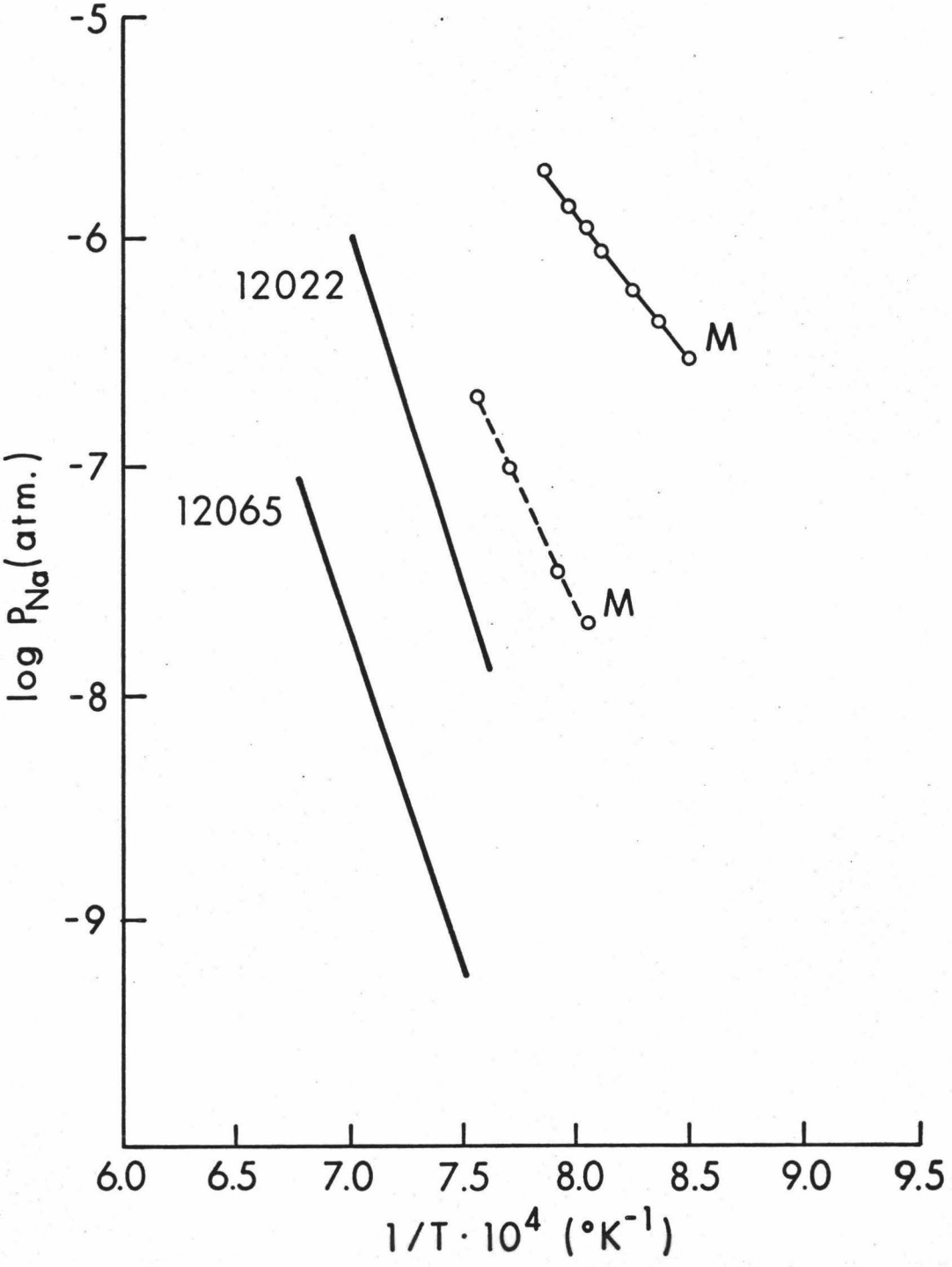

FIGURE 19 Sodium Vapor Pressure Comparison of Allende Carbonaceous Chondrite (M) With Lunar Basalts 12022 and 12065. Solid M line represents degassing; dashed M line is reheating of degassed residue.

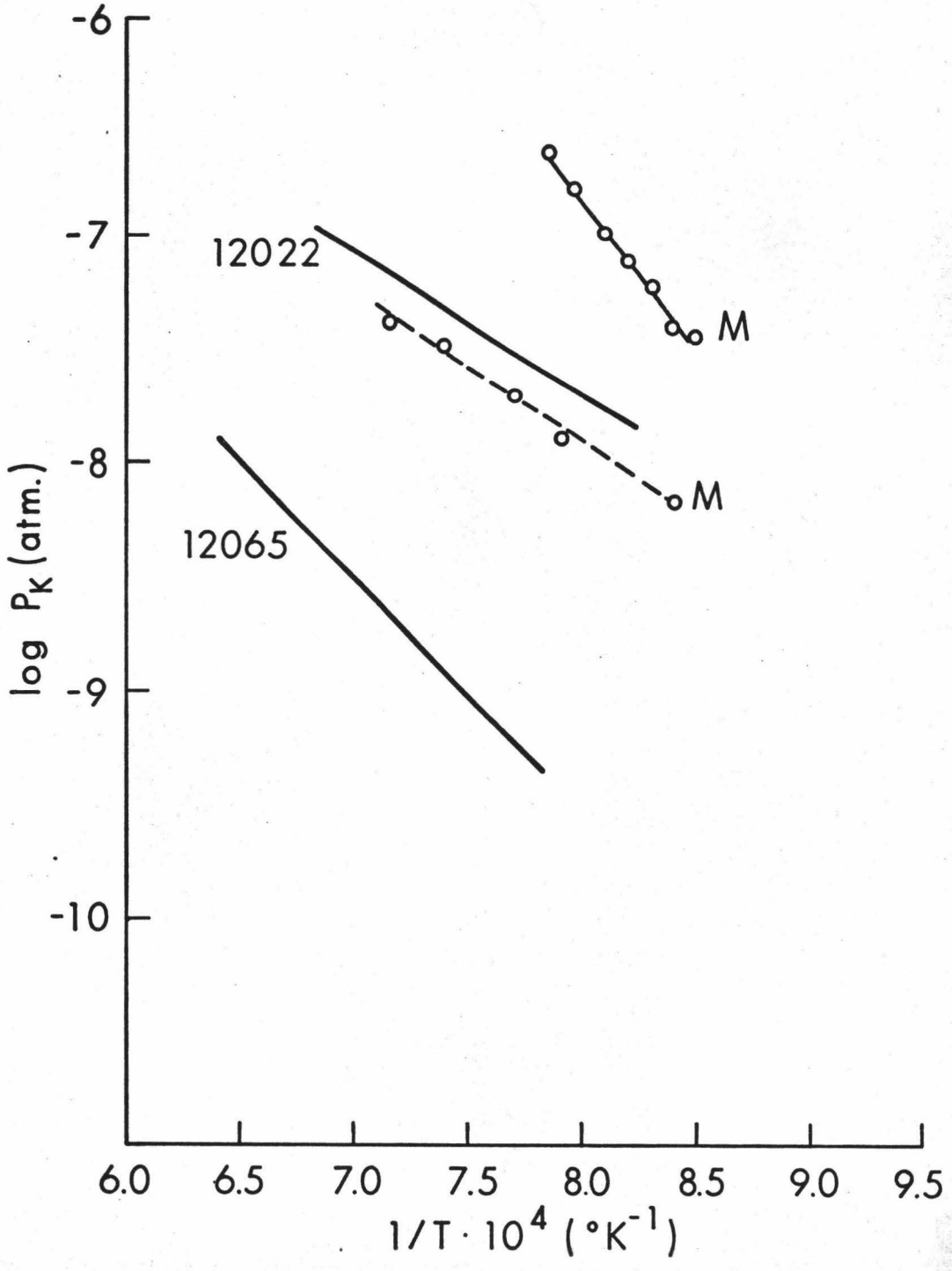

FIGURE 20 Potassium Vapor Pressure Comparison of Allende Carbonaceous Chondrite (M) With Lunar Basalts 12022 and 12065. Solid M line represents degassing; dashed M line is reheating of degassed residue.

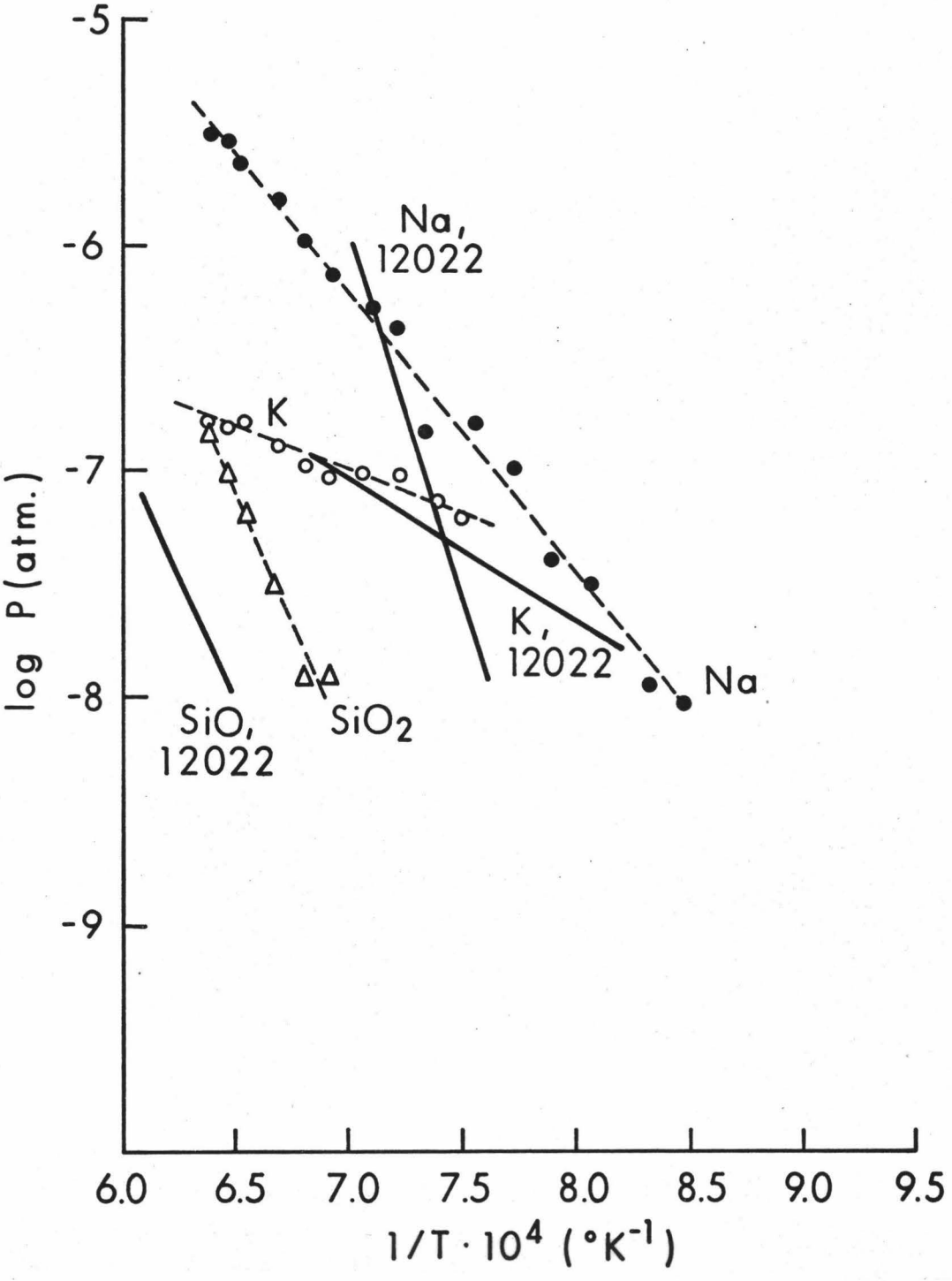

FIGURE 21 Sodium, Potassium and Silica Vapor Pressure Comparison of Plagioclase Feldspar (P) With Lunar Basalts 12022 and 12065. P is represented by dashed lines.

fusion runs (solid lines in Figure 17 and 18) produced non-linear plots which indicate the operation of a nonequilibrium vaporization process during degassing. It should be pointed out that the scatter of data points in the linear plots from this investigation is similar to that in the data of De Maria, et al. (1971) although, for clarity of presentation, the individual data points given by the latter workers have been omitted from Figures 17-21.

The data in Figures 17-21 supports that in Figures 15 and 16 by confirming the unusual alkali vaporization behavior which occurred during the vesiculation of the basalts in vacuum. No such perturbations were evident in the Clausius-Clapeyron plots for the tektites (T1 in Figures 17 and 18) and plagioclase feldspar (Figure 21). The results for sample M, the Allende meteorite, will be considered separately in a later discussion (see page 76).

Allowing for compositional differences which remain, the degassed terrestrial basalts exhibited the same vaporization trends as observed for the lunar basalts. During vesiculation, though, the anomalous manner of alkali vaporization from the terrestrial basalts distinguished them clearly from their lunar analogs. The implications of this behavioral contrast will be discussed in the next section.

It should not be overlooked that the high rates of Type I alkali vaporization from the basalts were possibly the result of chemical reactions. Accordingly, the information in Table 6 was compiled during a search for such a

Table 6

Hypothetical Alkali-Specific Chemical Reactions at 1000° C

Reaction	ΔG (kcal), P = 1 atm, M = Na	ΔG (kcal), P = 1 atm, M = K	ΔG (kcal), P = 10^{-9} atm, M = Na	ΔG (kcal), P = 10^{-9} atm, M = K
(1) $2\ FeS_{(s)} + 4\ M_2O_{(s)} \longrightarrow 2\ SO_{2(g)} + 8\ M^{o}_{(g)} + 2\ Fe^{o}_{(s)}$	130.98	62.39	-393.32	-461.91
(2) $FeS_{(s)} + 3\ M_2O_{(s)} \longrightarrow SO_{2(g)} + 6\ M^{o}_{(g)} + FeO_{(s)}$	76.81	25.37	-290.20	-341.64
(3) $FeS_{(s)} + 3\ M_2O_{(s)} + TiO_{2(s)} \longrightarrow SO_{2(g)} + 6\ M^{o}_{(g)} + FeTiO_{3(s)}$	72.09	20.69	-294.92	-346.32
(4) $S_{2(g)} + 4\ M_2O_{(s)} \longrightarrow 2\ SO_{2(g)} + 8\ M^{o}_{(g)}$	95.09	26.50	-376.78	-445.37
(5) $S_{2(g)} + 3\ M_2O_{(s)} + FeTiO_{3(s)} \longrightarrow 2\ SO_{2(g)} + 6\ M^{o}_{(g)} + TiO_{2(s)} + Fe^{o}_{(s)}$	88.45	37.01	-278.56	-330.00

- CONTINUED -

Table 6

(Continued)

	Reaction	ΔG (kcal), P = 1 atm, M = Na	ΔG (kcal), P = 1 atm, M = K	ΔG (kcal), P = 10^{-9} atm, M = Na	ΔG (kcal), P = 10^{-9} atm, M = K
(6)	$C_{(s)} + M_2O_{(s)} \longrightarrow CO_{(g)} + 2\ M^o_{(g)}$	3.22	-13.92	-154.07	-171.21
(7)	$CO_{(g)} + M_2O_{(s)} \longrightarrow CO_{2(g)} + 2\ M^o_{(g)}$	13.63	-3.51	-91.23	-108.37
(8)	$M_2O_{(s)} \longrightarrow 2\ M^o_{(g)} + \frac{1}{2}\ O_{2(g)}$	55.66	38.52	-75.42	-92.56
(9)	$2\ MAlSi_3O_{8(s)} \longrightarrow 2\ M^o_{(g)} + Al_2O_{3(s)} + 6\ SiO_{2(s)} + \frac{1}{2}\ O_{2(g)}$	140.66	145.01	9.58	13.94

Average uncertainties of ± 7% apply to the values of Δ G.
Details of the calculations are given in Appendix C.

set of alkali-specific reactions. Reactions were included in the tabulation on the basis of their consistency with the experimental evidence, prospective entries being screened on the basis of the following criteria:

(i) The reaction must involve only those chemical constituents which are normally present in basalts (see Table 1, page 2).

(ii) The reaction must produce the alkalis in the atomic forms Na° and K°.

(iii) The reaction must show the dependence of the alkali release on the chemical composition of the associated gas phase (see Table 5, page 60). The relative proportions of the reactants and products in the postulated reaction must agree with those observed experimentally and must be consistent with the initial composition of the basalt.

(iv) The reaction must possess a negative (or small positive) free energy change, ΔG, over the 900-1000° C range.

The preceding criteria can be effective in screening potential reactions if the full implication of each is understood. First, condition (i) requires that the reaction should be able to operate from any basalt of normal composition. Normal, in the present sense, means that the basalt possesses a typical eruptive composition and has undergone no metamorphism or other process which might have affected its volatile element content. The evaluation of

possible reactions should allow for the compositional differences between terrestrial and lunar basalts since the extension of data on the former to the case of the latter is of principal interest here.

Since the alkalis were vaporized from the basalts predominantly as the atomic species Na^{o} and K^{o}, condition (ii) requires that any plausible alkali-specific chemical reaction must explain their release in those forms. The alkalis exist almost certainly as ions in the melt, as will be further discussed, so that some reduction reaction must operate during vaporization. It is, of course, possible that the chemical reduction of the alkalis to neutral atoms may involve two or more reaction steps. However, coupled or multi-step reaction mechanisms are, in the context of this experimental study, inherently less appealing.

Condition (iii) is a pivotal one since the central working hypothesis, that the gases escaping from a molten basalt under high vacuum somehow influence the accelerated vaporization of alkalis, leads immediately to the question of how important to the phenomenon is the chemical composition of the gas phase. The experimental data show that SO_2 was the major gas which appeared with the alkali vapors (see Table 5, page 60). Thus, possible reactions in the melt between sulfur and the alkalis deserve special consideration although the participation of other elements must not be totally discounted. In any case, the stoichiometry of the postulated reaction (or set of reactions) should be

consistent with both the initial concentrations of all reactants in the melt and the final concentrations of all products in the gas phase.

Finally, condition (iv) requires that the postulated reaction be thermodynamically favorable over the experimentally studied range of 900-1000° C. The Gibbs free energy change, ΔG, obtained from thermochemical calculations depends crucially on the physical-chemical states which are assumed for the reactants and products. Accordingly, the values of ΔG for the reactions in Table 6 will vary depending on whether reactants are assumed to be solids (s) or liquids (l). Furthermore, the numerical entries in Table 6 demonstrate the influence of assumed total pressure on the computed values of ΔG. The methods of calculation are detailed in Appendix C.

Knowledge of the physical chemistry of basaltic liquids is still rather meager although it is accepted by most workers that the structures of such liquids are ionic in nature (Barth and Rosenqvist, 1949; Bockris and Lowe, 1954). Barth and Rosenqvist (1949) suggested that basaltic liquids consisted of SiO_4^{4-} ions in solution with, primarily, Ca^{2+}, Mg^{2+}, Fe^{2+}, Na^+, and K^+ ions. On the basis of the ionic model, then, the choices of Na_2O and K_2O as the forms of the alkali reactants in Table 6 would seem less realistic. However, the use of Na_2O and K_2O can be rationalized on the basis of (1) the need to accomodate the oxygen which is required for the formation of the presumed gaseous products

such as SO_2, and (2) the greater availability of thermochemical data for the oxides at elevated temperatures. Although it might seem reasonable to assume liquid (l) states for the reactants in Table 6, the more readily available thermochemical data for solids make the assumption of solid (s) states for the reactants preferable for purposes of consistency.

All factors considered, the entries in Table 6 represent the range of possible chemical reactions which best fit the screening criteria listed on page 70. Most of the reactions attempt to relate the alkali volatilization to the production of SO_2 (Reactions 1-5) or CO_2 (Reaction 7) while two consider the vaporization of alkalis as a first-order decomposition process (Reactions 8 and 9).

A principal feature of the set of reactions in Table 6 is their general increase in thermodynamic favorability with decreasing pressure. At 1 atm pressure, only Reactions (6) and (7) are favorable while in a vacuum of 10^{-6} torr ($\cong 10^{-9}$ atm) all but Reaction (9) are theoretically spontaneous processes. It is interesting that at 10^{-9} atm the volatilization of alkalis by chemical reaction with sulfur species (Reactions 1-5) or carbon species (Reactions 6 and 7) should be thermodynamically more favorable than their vaporization by simple decomposition of the rock (Reactions 8 and 9).

The assumptions made in compiling Table 6 should be recalled, however, before the results are overemphasized.

The difficulties involved in the assumption of $Na_2O_{(s)}$ and $K_2O_{(s)}$ as reactants have already been mentioned. Another difficulty is that if carbon exists in basaltic liquids as dissolved CO_2, i.e. CO_3^{2-} (Barth and Rosenqvist, 1949), then Reactions (6) and (7) are not plausible. The choice of FeS as a reactant is more defensible, though, since sulfide globules have actually been observed in basalts (Moore and Calk, 1971) and the existence of sulfur as S^{2-} has been confirmed for synthetic silicate glass melts at oxygen partial pressures of $P_{O_2} \leq 10^{-5}$ atm (Fincham and Richardson, 1954) which should be typical of both terrestrial basalts (Hamilton, et al., 1964) and lunar basalts (Nash and Hausel, 1973).

It is possible that chemical processes such as Reactions (2), (4), or (7) might have volatilized alkalis from the basalt samples which were studied in this investigation although the experimental evidence does not justify such a conclusion. The interpretation of such reactions in the context of lunar volcanism will be attempted in the next section (see page 78). In the case of the basalts used in this investigation, though, the accelerated vaporization of alkalis might be explained equally well in terms independent of alkali-specific chemical reactions.

The influence of viscosity and specific surface area on the rates of alkali vaporization from a basalt have already been mentioned. Basalts B1 and B2 had low specific surface areas (2% and 1% vesicles, respectively, Table 2,

page 8) but possessed high concentrations of gas-forming volatiles (Table 5, page 59) which produced vigorous agitation and vesiculation during melting. It is probable that the volatiles lowered the viscosity of the melt (Turner and Verhoogen, 1960, page 54; Scarfe, 1973) thereby increasing the activities of the alkalis it contained. Bubble formation and breakage disrupted the liquid structure and increased the specific surface area of the melt such that the alkalis were further mobilized, resulting in their nonequilibrium vaporization at accelerated rates. Basalts B3 and B4 both possessed higher initial specific surface areas (50% and 75% vesicles, respectively) and higher initial alkali concentrations than B1 and B2. Even though B3 and B4 contained less gas than B1 and B2 (see Table 5) their volatile contents were sufficient to produce appreciable vesiculation. Thus, their alkali vaporization rates are consistent with their placements relative to B1 and B2 in Figures 15 and 16. As a group, the basalts reflect the compositional control of vaporization in their Type II rates while the great importance of gas content and specific surface area is demonstrated by their Type I rates.

The tektites, T1 and T2, vaporized alkalis in conformity with the constraints of initial alkali concentration and viscosity since they did not vesiculate significantly and contained no alkali-rich mineral phases.

Plagioclase feldspar, P, showed alkali vaporization behavior consistent with diffusion-controlled thermal

decomposition. The very small gas content of the plagioclase made gas-induced alkali losses insignificant.

The Allende carbonaceous chondrite, M, presents a paradox since it exhibited anomalously high Type I alkali vaporization rates (see Figures 15 and 16) although the vaporization apparently occurred by equilibrium processes (see Figures 19 and 20). Volatilization of alkalis by chemical reaction might then seem a plausible explanation. The mass pyrogram in Figure 14 (page 46) shows that S_2, SO_2, and CO appeared in the gas phase during the vaporization of alkalis from the meteorite, suggesting that Reactions (1), (2), (4), or (6) in Table 6 might have been responsible for the pronounced alkali release from the sample. As seen in Table 6, all four postulated reactions have favorable free energy changes under the experimental conditions of 1000° C and 10^{-9} atm but only Reaction (6) approaches spontaneity at 1 atm pressure. The proposed reactants are realistic choices since both FeS and C are abundant in the meteorite (see Table 1, page 2) and, although the form of C is not well known (Clarke, et al., 1970), its presence as graphite is not precluded.

Clarke, et al. (1970) reported nepheline ($NaAlSiO_4$) and sodalite ($Na_4Al_3Si_3O_{12}Cl$) as rare accessory minerals in the Allende meteorite so that the thermal decomposition of one or both of those alkali-rich minerals could explain, in part, the high rates of alkali vaporization which were observed for the meteorite. However, their suggested rarity

leads to the retention of one or more of the postulated chemical reactions as the more likely explanation of the alkali vaporization behavior.

For the purposes of this project, the important conclusion to be drawn from the results of the vaporization experiments is that, under high vacuum conditions, gas-rich basaltic lava will lose alkalis by vesiculative vaporization and at rates significantly greater than those which would prevail in the absence of vigorous degassing.

B. Implications for Lunar Volcanism

The observations made in this investigation on the vaporization of molten basalts under high vacuum provide the basis for some commentary on two aspects of lunar volcanic history:

(1) The Na and K depletions in mare lavas and

(2) The growth of minerals from the vapor phase

1. The Na and K Depletions in Mare Lavas

The experimental results presented earlier indicate that the eruption into vacuum of a gas-rich lava should result in anomalously high alkali loss rates as vesiculation proceeds. Storey (1973) commented on the high alkali loss rates which he observed during the initial degassing of a terrestrial basalt under vacuum although his report did not include any information on the chemical

composition of the gases involved or the chemical forms of the vaporized alkalis.

Thus, vesiculative vaporization is undoubtedly a real phenomenon although its importance in controlling the bulk compositions of extruded lunar lavas has not been fully evaluated. Gibson and Hubbard (1972) allowed that bubbling or fountaining of lunar lavas may have resulted in higher rates of vaporization but they found no evidence for such behavior in their heating experiments on lunar rocks. Upon first consideration, then, it might seem that the mechanism for late-stage alkali depletion of lunar basalts has been identified in the present report as vesiculative vaporization. However, the following discussion is intended to show that even the greater alkali loss rates implied by the results reported here are not sufficient to explain the low alkali contents of lunar basalts.

The vesiculative vaporization process can be considered to be primarily either chemical or physical in nature. The chemical interpretation and its application will be discussed first. Upon reconsidering the data in Table 6, it might appear that all the reactions except Reaction (9) are capable of explaining the volatilization of alkalis from molten basalts in a vacuum of 10^{-9} atm. To extend these postulated reactions to the case of a lava flow on the Moon, however, requires recognition that only the surface of the flow would experience vacuum conditions. Due to the weight of the overlying lava the lithostatic pressure within the

flow would increase with depth, accompanied by the decrease in thermodynamic favorability of the postulated chemical reactions. Clearly, for each reaction in Table 6 there exists a critical pressure, P*, such that $\Delta G = 0$. At values of $P > P^*$ it follows that $\Delta G > 0$ and the reaction would not be favorable. Conversely, for $P < P^*$ the reaction should be spontaneous since $\Delta G < 0$. Choosing Reaction (2) as typical of the entries in Table 6, a critical pressure of $P^* = 0.013$ atm was calculated for the volatilization of Na using Equation (29) in Appendix C.

The depth in the lava flow at which a certain lithostatic pressure would prevail can be calculated from the barometric equation (Moore, 1962, page 230) as

$$h = \frac{P}{\rho g} \qquad (18)$$

where h is the depth (from the surface of the flow) at which pressure P prevails in a lava of density ρ experiencing a gravitational acceleration g. Assuming a lunar lava density of 3.0 g/cm^3 (Weill, et al., 1970) and a lunar gravitational acceleration of 1/6 that of the Earth, the critical depth for the volatilization of Na by Reaction (2) is found to be 0.27 mm [=((0.013 atm)(1 dyne cm^{-2}/9.869 x 10^{-7} atm)) ÷ ((3.0 g cm^{-3})(1/6)(981 cm sec^{-2})) = 0.027 cm]. According to this model, then, depths in the flow greater than 0.27 mm should render Reaction (2) ineffective in volatilizing Na. Computations show that similar critical

depths apply to the other reactions in Table 6. If the pressures in the gas bubbles of lunar lavas were 0.01-100 atm (Wellman, 1970) then only the uppermost skins of the lunar lava flows should have been subject to substantial alkali volatilization since the pressures required to produce bubbles at depth would be thermodynamically unfavorable with respect to the postulated chemical reactions.

The adequacy of chemical volatilization in explaining the alkali depletions is also doubtful on the basis of mass balance considerations. In terms of atomic ratios between reactants and products, Reaction (2) in Table 6 (page 68) would be the most efficient in volatilizing alkalis from the melt since it produces six gaseous alkali atoms for each sulfur atom which reacts. The transformation by volatilization of a basaltic lava of terrestrial composition to one of lunar composition would entail alkali depletions of approximately 2.00% to 0.50% Na_2O and 0.50% to 0.05% K_2O (see Table 1, page 2). Assuming that the volatilization was accomplished by Reaction (2), the sulfur requirements would be 0.26% S [= ((2.00 - 0.50 g Na_2O)/ 62.0 g gfw^{-1}))(1 S/3 Na_2O)(32.1 g S/gfw)] to volatilize the Na and 0.05% S [= ((0.50 - 0.05)/94.2))(1/3)(32.1)] to volatilize the K. The total required sulfur concentration of 0.31% [= 0.26 + 0.05] is greater than the 0.20% S observed for sulfur-saturated (at 1 atm) terrestrial mafic magmas (Haughton, et al., 1974) and also greater than the 0.2% S observed in samples of quenched pre-eruption melt which

were preserved as silicate inclusions in the phenocrysts of lunar basalts (Roedder and Weiblen, 1970). Thus, Reaction (2) alone is unlikely to account for the observed alkali depletions. However, if it is postulated that Reaction (7) on page 69 operated simultaneously with Reaction (2) then the chemical volatilization hypothesis might still be tenable. The amount of alkalis which could not be volatilized by Reaction (2) because of the sulfur deficiency would be 0.010 gfw Na_2O and K_2O [= ((0.31 - 0.20 g S/32.1 g gfw^{-1})) (3 M_2O/1 S)]. By the terms of Reaction (7), the alkali excess would translate to a carbon requirement of 0.28% CO [= (0.010 gfw M_2O)(1 CO/1 M_2O)(28.0 g·gfw^{-1})] or 0.12% C. The pertinent saturation value for a basic magma at 3000-5000 atm pressure is ≤ 0.6% CO_2 (Khitarov and Kadik, 1973) which is equivalent to 0.16% C. Thus, the lunar lava would need to be saturated with both sulfur and carbon in order for the chemical volatilization of alkalis to proceed with the efficiency required to account for the alkali depletions in the residual rocks. As pointed out earlier, though, the volatilization effects would, in any case, probably be limited to the thin interface between the surface of the flow and the lunar vacuum.

Essentially the same conclusion can be reached empirically using the experimental data presented earlier and assuming vesiculative vaporization to be a purely physical effect. The observations made during this investigation have shown that accelerated rates of alkali vaporization

occur during the vigorous vesiculation of molten basalts under high vacuum but that once degassed the residual basalts release alkalis by a more predictable thermal decomposition mechanism. By analogy, it might be inferred that the rates of alkali loss from lunar lavas would consist of contributions from both the thermal decomposition and vesiculation mechanisms.

An estimate of the thermal decomposition contribution can be drawn from the data of Gibson and Hubbard (1972). They reported 1824 ppm Na and 536 ppm K in the initial aliquots of lunar basalt 12022 at the start of their vaporization study and observed 1200 ppm Na and 300 ppm K in the same aliquots after 2 hr of heating at 1200° C under vacuum. Those results imply thermal decomposition rates at 1200° C of 312 μg Na/g/hr [= (1824 - 1200)/2] and 118 μg K/g/hr [= (536 - 300)/2]. The measurements of vesiculative vaporization rates made in this study were confined by the vesiculation process itself to the 900-1000° C range so that they do not reflect the rates to be expected at 1200° C. But there is no reason so expect that vesiculation at 1200° C would be any less effective than vesiculation at 1000° C so that if it is assumed that the ratio of vesiculative to thermal decomposition vaporization rates is the same at both 1200° C and 1000° C then the data from this investigation suggest that vesiculative vaporization rates for gas-rich lunar lavas would be approximately three times greater than their thermal decomposition rates (sample B2, Figures 15,16).

Implicit in the analogy is, again, the assumption that the abundance of gases in terrestrial lavas represents the upper limit of gas concentrations to be expected in lunar lavas.

From the above it may then be postulated that the extrusion into vacuum of a lunar lava having the composition of rock 12022 would, at 1200° C, result in alkali loss rates of 3 (312) = 936 μg Na/g/hr and 3 (118) = 324 μg K/g/hr as vesiculation occurred. To explore the possibility that lunar basalt 12022 was derived from a lava with initial alkali concentrations equal to those of basalt B2 but which suffered large-scale vaporization losses, the extrapolation of the data for B2 and 12022 indicates that 16.4 hr [= (17,200 - 1824)/936] and 9.6 hr [= (3650 - 536)/324] would be required to reduce the Na and K concentrations, respectively, to the desired final values. However, the high rates of alkali vaporization would operate only as long as vesiculation occurred. Once degassing had been accomplished the rates would decrease by a factor of three and much longer times would be required to achieve the same depletion effects.

For a lava similar to B2 to be transformed by vaporization losses into rocks such as 12022 implies that, in the hypothetical limiting case, a 10-20 hr supply of gas and thermal energy must be available to keep the lava vesiculating vigorously at 1200° C. Only an active lava lake could approach such stringent requirements. Biggar, et al. (1971) suggested that petrogenesis of the presently

observed alkali-poor lunar basalts had occurred in lava lakes but it seems, on the basis of the preceding discussion, that unusually efficient convection would be required in order to expose the entire volume of the lake to the vacuum at the surface and thereby homogenize its alkali concentrations. More likely, convection in the lava lakes would be less than 100% efficient so that deep regions would suffer less alkali depletion than the shallow regions.

The compositions of all lunar basalts returned to Earth thus far show virtually the same low concentrations of Na and K. These include basalts which were apparently excavated from the lunar bedrock by impact events (Lunar Sample Preliminary Examination Team, 1972) and samples of quenched pre-eruption melt which were preserved as silicate inclusions in phenocrysts (Roedder and Weiblen, 1970). Furthermore, the exposed strata at Hadley Rille (Howard et al., 1972) indicate that individual lava flows of about 10 m thickness, rather than lava lakes, may have been the fundamental units involved in the filling of the mare basins. Thin flows should degas and cool in times much shorter than those needed to explain the depletion of alkalis by vesiculative vaporization. While it is not difficult to imagine the occurrence of lava lakes on the Moon it is doubtful that they controlled the bulk chemical compositions of all mare basalts.

Localized vaporization losses during vesiculation, which may have included chemical volatilization effects,

can probably account for some anomalies in certain lunar basalts (Brown and Peckett, 1971; Brown et al., 1972) but the uniformly low alkali concentrations of the basalts, in general, were probably not controlled by vaporization of their parent lavas under vacuum. Instead, the low alkali concentrations are almost certainly primary effects, reflecting either petrogenesis of the basalts from alkali-poor source materials (Ringwood and Essene, 1970; Gast et al., 1970) or the retention of alkalis by a separate and thus far undiscovered nonmare material (Rhodes and Hubbard, 1973).

(2) Growth of Minerals from the Vapor Phase

The experimental results presented earlier have shown that vesiculation of gas-rich molten basalts under high vacuum produces a gas phase which is rich in the alkalis Na and K. Even though the preceding discussions have demonstrated that such vaporization would not significantly alter the bulk composition of the lava, the experimentally verified existence of such an alkali-rich vapor phase under the conditions which would be expected during a lunar volcanic eruption clearly supports the concept of a vapor phase origin for the filamentary plagioclase crystals found in the vugs of lunar basalts (Skinner and Winchell, 1972). If lunar basalts were extruded initially at 1100-1200° C (Roedder and Weiblen, 1970) while the requisite alkali-rich vapors exist at temperatures as low as 900-1000° C (as the results from this project indicate) the inference that crystal growth

occurred in the lunar vugs after the lava had largely congealed (Skinner and Winchell, 1972) seems to be substantiated. Since no significant mobilization of Ca, Al, or Si by vesiculative vaporization was observed it is further assumed, in agreement with Skinner and Winchell (1972), that the growth process of the plagioclase druses employed Ca, Al, and Si which were derived from the immobile host rock. The last assumption gains support from the fact that crystallization of the mixed Ca-Na-K feldspar would probably proceed by pathways similar to the reverse of Reaction (9) (page 69) and be thermodynamically favorable at 1000° C. CaO from the host rock might substitute for the required O_2.

It is possible that vesiculation of lava at higher temperatures may have similarly activated the vaporization of Fe such that its deposition from a sulfur-rich vapor phase resulted in the FeS druses observed in lunar rocks (Carter, 1973). Since the work in this project included observation of the behavior of a sulfur-rich gas phase from basaltic melts for which no such anomalous vaporization of Fe occurred, it is concluded that impact events are more likely sources of the FeS lunar whiskers (Carter, 1973) than are volcanic events.

In discussing the vapor deposition of alkali-rich minerals in vugs, the influence of gas phase composition should be considered. The vesicular and vuggy textures of lunar basalts attest to the presence of gases during their formation although the composition of the gas phase which

attended the lavas remains one of the most intriguing mysteries in lunar science. Gas-release studies of lunar basalts (Gibson and Johnson, 1971) revealed that CO, CO_2, H_2S, and SO_2 were principal species at high temperatures, suggesting that a gas phase similar to that proposed by Wellman (1970) may have formed the vesicles. The gas phase which led to the vesiculation of the basalts in the experiments reported here was also dominated by carbon and sulfur gases, although H_2O was more abundant in the terrestrial samples than in the lunar samples.

Petrologic arguments seem to favor nearly anhydrous magmas as the progenitors of lunar basalts (Smith et al., 1970) although detection by the Apollo SIDE experiment of an apparent degassing event on the lunar surface (Freeman, et al., 1972) sustains the possibility that juvenile H_2O may exist at depth in the Moon. In either case, it does not seem likely that the presence or absence of H_2O would have significantly affected the formation of alkali-rich vapor phases from lunar lavas. The experimental results from this work have shown that the alkalis are transported principally as the atoms Na and K and in no way rely on the formation of NaOH, KOH, or similar volatile compounds for their mobility. Thus, the role of H_2O in both the experimental case and the analogous lunar case would only be to provide additional agitation of the melt. The formation of other volatile compounds such as NaCl or KCl might further facilitate the entrance of the alkalis into the vapor phase but

certainly are not required to explain the observations made during these experiments.

If the Moon accreted from material which was similar in composition to the Allende meteorite (Anderson, 1973) then the gas phase generated from a sample of the meteorite in this investigation may closely resemble the gas phase which vesiculated the lunar basalts. It is not impossible that some of the alkali-specific chemical reactions (pages 68-69) discussed earlier may have operated in the formation of the lunar volcanic vapors although further experimental work is needed to evaluate the prospects for such reactions, especially with respect to the influence of pressure and chemical state of the reactants and products.

At present it appears that the derivation of alkali-rich vapors from lunar lavas was a process which was more dependent on the volume of available magmatic gas than on its chemical composition, although it is still likely that the gases were rich in carbon and sulfur species. The movement of alkali-rich vapors through the vesicles and vugs of lunar basalts was probably a common feature of lunar volcanism in the past, such vapors almost certainly being parental to the filamentary plagioclase crystals which have been preserved in the vugs of some rocks.

IV. CONCLUSIONS

The high-temperature vacuum vaporization of selected samples of Hawaiian basalts, plagioclase feldspar, tektites, and the Allende carbonaceous chondrite have been studied by Knudsen cell-quadrupole mass spectrometry. Vaporization of the sample materials occurs principally by thermodynamically-controlled decomposition. It was found that the abundant gas-forming chemical species in both the basalts and the meteorite significantly increases their alkali vaporization rates during degassing. The gas-induced alkali losses appear to result from increases in the chemical activities of the alkalis. In the case of the basalts, the increase in alkali activities is due to the disruption of the liquid structure and an increase in specific surface area which occurs during vigorous agitation of the melt undergoing bubbling. Chemical volatilization by reaction of Na_2O and K_2O with carbon and sulfur species may also occur in vacuum although such reactions would be thermodynamically unfavorable at 1 atm pressure. Alkali-specific chemical reactions are the more likely explanations for activated alkali release from the meteorite.

Extension of knowledge about the vesiculative vaporization of Na and K from molten terrestrial basalts under high vacuum leads to the expectation that similar anomalously high alkali vaporization rates would be typical of freshly erupted lunar lavas. The principal result of such behavior

would be the formation of alkali-rich vapors and their transport by a carrier phase of carbon and sulfur gases through the vugs and vesicles of congealing lunar basalts. It is conceivable that such alkali-rich vapors could deposit plagioclase microcrystals in vesicles and vugs by reaction with the host rock.

The mobilization of alkalis into the vapor phase during lunar volcanic events would be comparatively large but probably not of sufficient magnitude to account for the conspicuosuly low concentrations of Na and K in lunar basalts. It is not likely that vaporization processes during eruption could have transformed a basalt of terrestrial composition into one of lunar composition. Thus, the alkali depletions in lunar basalts must be primary petrogenetic features.

APPENDIX A

Operating Instructions For Quadrupole Mass Spectrometer System

I. Vacuum System (Refer to Figure 3, page 17)

A. Establishing Vacuum from a Start at 1 atm

(1) Verify that VacIon pump isolation port is completely CLOSED.

(2) Set VacIon control switch to START position. (If the VacIon pump was already in operation this step is unnecessary and the switch should be left in the PROTECT position).

(3) Verify that the full weight of the bell jar is properly seated on the Viton gasket. Check to see that no part of the glove bag is caught in the seal.

(4) START FOREPUMP. Wait for initial pump noise to subside.

(5) Verify that vacuum system bleed valve is completely CLOSED.

(6) Carefully OPEN Forepump Isolation Valve. The valve should be opened slowly to prevent disturbance of the sample in the Knudsen cell by the outrush of air.

(7) Switch ON Thermocouple Pressure Gauge. Wait for system pressure to decrease to $\leq$ 1 micron ($= 10^{-3}$ torr).

(8) Switch ON Ionization Gauge. Wait for ultimate forepump pressure of 2×10^{-5} torr to be achieved. (Depending on the cleanliness of the system, the ultimate forepump pressure may be achieved in 1-2 hr.

(9) OPEN SLIGHTLY the Water Cooling Valve. Verify that a steady, moderate rate of water flow is obtained.

(10) Switch ON Front and Side Fans on vacuum housing exterior.

I. Vacuum System

A. Vacuum from Start at 1 atm (--Continued--)

(11) Verify that the Titanium Sublimation Pump (TSP) Filament Adjust control is at 0.

(12) Set TSP Filament Selector to C and set the Percent On control to 100.

(13) Switch TSP Main Power ON.

(14) Increase Filament Adjust control setting until a current of 40 amp registers on the TSP AC ammeter.* Observe pressure increase on Ionization Gauge and maintain 40 amp current until pressure begins to decrease. Reduce Filament Adjust control to 0.

(15) Move Filament Selector switch to B. Repeat step (14).

(16) Move Filament Selector switch to A. Repeat step (14)but maintain 40 amp current.

(17) Maintain TSP filament current at 40-45 amp until a system pressure of 2×10^{-5} torr is achieved.

(18) CLOSE Forepump Isolation Valve.

(19) Maintain TSP filament current at 40-45 amp until the system pressure decreases to 2×10^{-6} torr. (Depending on the cleanliness of the system, the time required to reach this pressure may vary from 5 to 90 min.

(20) Set VacIon control switch to PROTECT.

(21) Slowly OPEN VacIon Isolation Port while watching the VacIon meter (set in PRESSURE mode) to ensure that a pressure of 2×10^{-7} torr is not exceeded.

(22) When VacIon Isolation Port is fully OPEN, degas Ionization Gauge then re-check system pressure which should be $\leq 2 \times 10^{-7}$ torr.

(23) Reduce TSP filament current to desired setting (usually ≤ 40 amp).

---

* If no current flow is obtained, reduce Filament Adjust to 0 and proceed to steps (15) or (16) as required to establish filament current.

I. Vacuum System

B. Establishing Vacuum from Forepump Pressure

Perform steps (8)-(23) in Section I-A.

II. High-Temperature Mass Spectrometer System

CAUTION: DO NOT OPERATE MASS SPECTROMETER AT PRESSURES $\geq 10^{-6}$ TORR.

A. Quadrupole Mass Analyzer

(1) Switch ON Sorenson ACR 1000 power regulator and allow a few seconds for stabilization.

(2) Switch Recorder ON.

(3) Set QUAD Mode switch to SCAN.

(4) Turn QUAD Power switch ON. Wait for appearance of sine wave trace on oscilloscope.

(5) Turn Pre-amp switch ON. (Pre-amp switch is located on panel below VacIon pump). The QUAD oscilloscope sine wave should now become a flat horizontal baseline.

(6) Switch QUAD S.E.M. Voltage control ON and rotate to maximum clockwise position.

(7) Set Quad Filament switch to position 1 or 2 (Filament 2 gives maximum sensitivity). A momentary current pulse will appear on the Emission/AMU meter.

(8) Slowly adjust QUAD Emission control until desired filament current is registered on the Emission/AMU meter when set in the EMISSION CURRENT position. (Typically, 0.4-0.5 mA is optimum).

(9) Set QUAD Scan Speed switch to 0.1 position. A mass spectrum should be apparent on the QUAD oscilloscope.

(10) Switch ON external storage oscilloscope, if desired.

(11) Allow 30 min for stabilization of system before beginning analytical work.

II. High-Temperature Mass Spectrometer System

B. Spectral Range Adjustments

(1) Set Mode switch to SCAN.

(2) Switch Emission Current/AMU control to AMU position.

(3) Hold QUAD momentary-type Scan switch in START position.

(4) Alternately adjust Mass Range and Center Mass controls until the mass number of the low end of the desired spectral range is indicated on the Emission Current/AMU meter.

(5) Hold Scan switch in END position.

(6) Alternately adjust Mass Range and Center Mass controls until the mass number of the high end of the desired spectral range is indicated.

(7) Repeat steps (2)-(5) as required to obtain the desired mass range.

(8) Return Emission Current/AMU switch to EMISSION CURRENT position.

(9) Adjust Resolution control to desired setting. (Because of the inverse relationship between resolution and sensitivity, it is best to determine the optimum Resolution control setting by trial and error and then, once established, leave fixed.)

C. Spectral Scanning

(1) Set Mode switch to SCAN.

(2) Set Scan Speed switch to desired setting. (Position 60 is convenient for a mass range of about 60-70 amu and a chart speed of 2 in/min).

(3) Hold Scan switch in START position.

(4) Switch Recorder Drive ON.

(5) Release Scan switch.

(6) When scan is completed, switch Recorder Drive OFF and return Scan Speed control to 0.1.

II. High-Temperature Mass Spectrometer System

D. Peak Monitoring

(1) Switch Emission Current/AMU control to AMU.

(2) Set Mode switch on MANUAL.

(3) Adjust Center Mass control until the mass number of interest is registered on the Emission Current/AMU meter. Adjust Center Mass control until maximum vertical signal is obtained on the oscilloscope.

(4) Switch Recorder Drive ON and monitor as desired.

E. Knudsen Cell Operation

CAUTION: DO NOT OPERATE AT PRESSURES $\geq 10^{-6}$ TORR

(1) Switch Digital Temperature Indicator ON.

(2) Verify that Variacs 1 and 2 are OFF and that Variac 2 is set at 0. (Note: Variac 1 is usually pre-set at 60-80).

(3) Switch Variac 1 ON. Switch Variac 2 ON.

(4) Carefully adjust Variac 2 until 1 volt registers on the voltmeter.

(5) Following the temperature-voltage calibration curve, establish a heating program at rates of 1-20° C/min as desired.

CAUTION: DO NOT EXCEED 10.5 V APPLIED VOLTAGE AND/OR 1400° C UNLESS THE SYSTEM HAS BEEN SPECIALLY MODIFIED TO ACCOMODATE EXTRA THERMAL AND ELECTRICAL STRESSES.

(6) When heating program has been completed, reduce Variac 2 to 0 and switch both Variacs 1 and 2 OFF.

(7) Verify that step (6) has reduced the applied voltage reading to 0 and that the registered cell temperature has begun to fall.

(8) Maintain vacuum of $\leq 10^{-6}$ torr until Knudsen cell has cooled to $\leq 50°$ C.

III. Sample Introduction and Retrieval

(1) Verify that the Knudsen cell heating circuit (Variacs 1 and 2) is OFF and that the Knudsen cell is at $\leq 50^{\circ}$ C.

(2) Verify that Forepump Isolation Valve is CLOSED.

(3) Verify that ALL QUAD MASS ANALYZER COMPONENTS ARE OFF.

(4) Verify that the Titanium Sublimation Pump is OFF and is at ambient temperature. (After operation, the TSP requires about 2 hr of cooling under vacuum).

(5) Verify that the water cooling circuit is OFF.

(6) Place the sample and/or cell liner which is to be introduced) inside the glove bag.

(7) Flush the air from the glove bag by inflating it with high-purity nitrogen gas.

(8) Gently squeeze glove bag to expel nitrogen.

(9) Repeat steps (7) and (8) twice.

(10) Verify that VacIon Isolation Port is completely CLOSED.

(11) Switch ON Ionization Gauge.

(12) Switch ON Thermocouple Pressure Gauge.

(13) Through the Bleed Valve (Figure 3, page 17), carefully introduce high-purity nitrogen into the vacuum system. A controlled bleed rate amounting to a factor of 10 pressure increase every 5 sec (e.g. 10^{-8} to 10^{-7} torr in the first 5 sec, 10^{-7} to 10^{-6} torr in the next 5 sec, etc.) should safely pressurize the system without disturbing any sample which might already occupy the Knudsen cell. (Note: Ionization Gauge will automatically switch OFF when a pressure of $\geq 10^{-4}$ torr is reached).

(14) When the Thermocouple Pressure Gauge registers 1 atm (1000 microns), increase nitrogen flow rate until the bell jar lifts slightly and the glove bag begins to inflate. Continue the nitrogen flow.

(15) Carefully raise the bell jar by means of the wench.

III. Sample Introduction and Retrieval (--Continued--)

(16) Attach safety line to bell jar and lock wench in place with both the hoist line and safety line slightly taught.

(17) Exchange samples and/or cell liners in the Knudsen cell by operation through the glove bag.

(18) Stop nitrogen gas flow.

(19) Detach bell jar safety line and carefully lower the bell jar until the glove bag is sufficiently deflated to allow proper seating of the Viton seal.

(20) Verify that no part of the glove bag is caught in the Viton seal.

(21) Verify that the corresponding alignment marks on the bell jar and lower vacuum housing exteriors are properly matched.

(22) Re-establish vacuum according to instructions in Section I-A.

APPENDIX B

Conversion of Mass Spectral Peak Heights To Ion-Currents

The relationship between mass peak height (H_i) and ion-current (I_i^+) for a specie i was given on page 31 as

$$I_i^+ = \left(\frac{1}{C}\right)\left(\frac{1}{I_x}\right)\sum\left(\frac{H_i}{G\,T_q}\right) \qquad (13)$$

The general form of Equation (13) can be explained as follows. A chemical specie such as an atom or molecule has an ionization efficiency, I_x, which is independent of subsequent fragmentation effects. The summation term in H_i allows for the general case where specie i is a molecule which, upon ionization, fragments into several daughter ions which appear in the spectrum at various mass numbers below that of the parent ion. Since electron multiplier gain, G, and quadrupole transmission efficiency, T_q, both decrease with increasing ion mass (Grimley, 1967; Rüdenauer, 1972) each fragment ion will possess its own set of G and T_q values. Hence, the peak heights of all fragment ions must be appropriately corrected and summed to give the total ion-current for specie i. Isotope peaks are included in the fragmentation pattern so that the isotopic abundance, C, is not explicitly included in the calculation.

For a monatomic specie such as Na^+, K^+, or Mg^+ the isotopic abundance is included as shown in Equation (13) with

the further simplification that the summation reduces to a single term since no fragmentation occurs. In that case, Equation (11) on page 29 can be combined with Equation (13) to give

$$f_i = \frac{I_i^+}{H_i} = (C\ I_x\ G\ T_q)^{-1} \qquad (19)$$

The substitution of Equation (19) into Equation (12) on page 29 leads to Equation (14) which is given on page 31.

Since quantitative analyses were performed only for Na, K, and Mg in this investigation, Equation (19) was used to compute the peak height-to-ion-current conversion factors.

The values of I_x, G, and T_q which were used to evaluate Equation (19) for the different species are given in Table 7. The isotopic abundances, C, were those given by Roboz (1968). For species other than Na, K, and Mg Equation (13), with the modifications discussed previously, was used to calculate I_i^+.

The ionization efficiency, I_x, of an atom or molecule is a measure of its ionization cross-section. Most previous mass spectrometric quantitative studies have employed the cross-section values compiled by Otvos and Stevenson (1956) but in this investigation it was decided to use I_x values derived from an empirical relationship proposed by Flaim and Ownby (1971). The latter workers demonstrated that the ionization efficiencies of gaseous species could be plotted as a linear function of the number of electrons per molecule.

Table 7

Values of Parameters
Used in Quantitative Analytical Calculations

Specie	m/e	I_x [a]	G [b]	T_q [c]
H_2	2	0.48	3.741	1.00
H_2O	18	0.82	1.247	1.00
F	19	0.82	1.214	1.00
Na	23	0.87	1.103	0.90
Mg	24	0.91	1.080	0.90
N_2	28	1.00	1.000	0.80
CO	28	1.00	1.000	0.80
O_2	32	1.09	0.935	0.80
H_2S	34	1.17	0.907	0.75
Cl	35	1.13	0.800	0.75
HCl	36	1.17	0.882	0.75
K	39	1.22	0.847	0.70
CO_2	44	1.35	0.798	0.65
(SO^+)	48	-	0.764	0.60
NaCl	58	1.61	0.695	0.55
SiO_2	60	1.70	0.683	0.55
Na_2O	62	1.70	0.672	0.55
S_2	64	1.78	0.661	0.55
SO_2	64	1.78	0.661	0.55
KCl	74	1.96	0.615	0.35
K_2O	94	2.39	0.546	0.30

[a] I_x values normalized to $I_x(N_2) = 1.00$.

[b] G values normalized to $G(N_2) = 1.00$

[c] T_q values estimated from those given by Bunyard (1973).

The data of Flaim and Ownby (1971) permitted the derivation of the empirical equation

$$I_x = 0.61\ N_e + 0.39 \qquad (20)$$

where N_e is the number of electrons per molecule divided by 14. Division by 14 normalizes the values to $I_x = 1.00$ for nitrogen. Since the mass spectrometer sensitivity was optimized on m/e = 28 (N_2^+) before the start of each analytical run it was reasonable to normalize the I_x values to that of N_2. Equation (20) was used to calculate the set of I_x values which are given in Table 7.

Electron multiplier gain, G, is related to ion mass, m, as $G \propto m^{-\frac{1}{2}}$ (Grimley, 1967). Accordingly, the set of G values in Table 7 were normalized to G = 1.00 for N_2.

The quadrupole transmission efficiency, T_q, is the ratio of the sample beam ion-current intensities at the exit and entrance points of the mass filter. An inverse relationship exists between T_q and the mass number, m, which Rudenauer (1972) suggests is $T_q \propto 1/m$. However, the values of transmission efficiency which were assumed in this study were taken from estimates given by Bunyard (1973).

APPENDIX C

Calculation of Free Energy Changes For Alkali-Specific Chemical Reactions At 1000° C

The Gibbs free energy change, ΔG, for each reaction in Table 6 (pages 68-69) was computed according to

$$\Delta G_T = T \cdot \Delta(fef)_{rxn} + (\Delta H^\circ_{298})_{rxn} \qquad (21)$$

where $(fef) = (G_T - H^\circ_{298})/T$ and is the free energy function referenced to 298° K (Lewis and Randall, 1961, page 166). All calculations were made for T = 1273° K. The values of (fef) at 1273° K for the various reactants and products were interpolated from data given in standard compilations. The interpolated data and references to their sources are listed in Table 8.

Two sets of ΔG calculations were made. The first, for P_{total} = 1 atm, used the data in Table 8 for direct computation by Equation (21). The second set of calculations, for $P_{total} = 10^{-9}$ atm, used the data in Table 8 and a modified form of Equation (21) which was derived as follows.

Each reaction in Table 6 can be represented in the general form

$$a\,A_{(s)} + b\,B_{(s)} + c\,C_{(s)} \longrightarrow x\,X_{(s)} + y\,Y_{(g)} + z\,Z_{(s)} \qquad (22)$$

where the reactants and products are both mixtures of gases and solids. If the gases are assumed to exhibit ideal

Table 8

Thermochemical Data at 1273° K for Selected Chemical Species

Substance	$-(G_T - H^\circ_{298})/T$, cal/mole/° K	ΔH°_{298}, kcal/mole	Reference[a]
$Na_2O_{(s)}$	31.61	-99.40	(1)
$Na^\circ_{(g)}$	40.12	25.76	(1)
$NaAlSi_3O_{8(s)}$ (high albite)	97.83	-934.51	(3)
$K_2O_{(s)}$	38.19	-86.80	(1)
$K^\circ_{(g)}$	41.70	21.31	(1)
$KAlSi_3O_{8(s)}$ (microcline)	95.38	-946.26	(3)
$FeO_{(s)}$	22.51	-63.8	(2)
$FeS_{(s)}$	25.85	-22.72	(2)
$Fe^\circ_{(s)}$	11.60	0	(2)
$FeTiO_{3(s)}$	44.22	-295.55	(2)
$TiO_{2(s)}$ (rutile)	22.94	-225.50	(1)
$SiO_{2(s)}$ (quartz)	19.78	-217.50	(1)
$Al_2O_{3(s)}$	29.05	-400.4	(2)
$S_{2(g)}$	60.23	30.84	(1)
$SO_{2(g)}$	64.76	-70.96	(2)
$C_{(s)}$ (graphite)	3.77	0	(2)
$CO_{(g)}$	50.41	-26.42	(2)
$CO_{2(g)}$	56.50	-94.05	(2)
$O_{2(g)}$	52.40	0	(2)

-- Continued --

Table 8

(Continued)

---

[a] References:

(1) Stull (1965).

(2) Lewis and Randall (1961), Appendix 7.

(3) Robie and Waldbaum (1968).

behavior under the conditions $P = 10^{-9}$ atm and $T = 1273^{\circ}$ K then the free energy of each gaseous component will be given by

$$G_T = G^{\circ} + RT \ln\left(\frac{P}{P^{\circ}}\right) \tag{23}$$

where G° is the free energy at $P^{\circ} = 1$ atm (Lewis and Randall, 1961, page 171). Neglecting the effect of pressure on the free energies of the solid components, the free energy change for Reaction (22) can be written as

$$\Delta G = x\left(G_X^{\circ} + RT \ln\left(\frac{P}{P^{\circ}}\right)\right) + y\left(G_Y^{\circ} + RT \ln\left(\frac{P}{P^{\circ}}\right)\right) + z\, G_Z^{\circ} - a\, G_A^{\circ} - b\, G_B^{\circ} - c\left(G_C^{\circ} + RT \ln\left(\frac{P}{P^{\circ}}\right)\right) \tag{24}$$

By collecting terms, Equation (24) can be simplified to read

$$\Delta G = x\, G_X^{\circ} + y\, G_Y^{\circ} + z\, G_Z^{\circ} - a\, G_A^{\circ} - b\, G_B^{\circ} - c\, G_C^{\circ} + (x + y - c)\left(RT \ln\left(\frac{P}{P^{\circ}}\right)\right) \tag{25}$$

which reduces to

$$\Delta G = \Delta G^{\circ} + (x + y - c)\left(RT \ln\left(\frac{P}{P^{\circ}}\right)\right) \tag{26}$$

For $P^{\circ} = 1$ atm, $P = 10^{-9}$ atm, and $T = 1273^{\circ}$ K it is found that $RT \ln (P/P^{\circ}) = (1.987)(1273)(2.303)(-9) = -52.43$ kcal.

Thus, the free energy changes for the reactions at $P = 10^{-9}$ atm were computed as

$$\Delta G = \Delta G^{\circ} + (x + y - c)(-52.43) \text{ kcal} \qquad (27)$$

Equation (26) can be rearranged to the form

$$\log P = \frac{(\Delta G) - (\Delta G^{\circ})}{(x + y - c)(2.303)(RT)} + \log P^{\circ} \qquad (28)$$

The pressure at which $\Delta G = 0$ for a selected reaction can then be evaluated as

$$\log P^{*} = \frac{-(\Delta G^{\circ})}{(x + y - c)(2.303)(RT)} \qquad (29)$$

where P^{*} is the critical pressure which corresponds to $\Delta G = 0$ for the case of $P^{\circ} = 1$ atm.

REFERENCES

Anderson, D. L. (1973) The composition and origin of the moon, Earth Planet. Sci. Lett., 18, 301-316.

Barth, T. F. W. and Rosenqvist, T. (1949) Thermodynamic relations of immiscibility and crystallization of molten silicates, Am. J. Sci., 247, 316-323.

Biggar, G. M., O'Hara, M. J., Peckett, A., and Humphries, D. J. (1971) Lunar lavas and the achondrites: petrogenesis of protohypersthene basalts in the maria lava lakes, Proc. Sec. Lunar Sci. Conf., 1, 617-643, M. I. T. Press.

Bockris, J. O'M. and Lowe, D. C. (1954) Viscosity and structure of molten silicates, Proc. Royal Soc. (London), A226, 423-435.

Brown, G. M. and Peckett, A. (1971) Selective volatilization on the lunar surface: evidence from Apollo 14 feldspar-phyric basalts, Nature, 234, 262-266.

Brown, G. M., Emelius, C. H., Holland, J. G., Peckett, A., and Phillips, R. (1972) Petrology, mineralogy and classification of Apollo 15 mare basalts, The Apollo 15 Lunar Samples, J. W. Chamberlain and C. Watkins (eds.), 40-44, Lunar Science Institute.

Brownlee, D., Bucher, W., and Hodge, P. (1972) Whiskers on the moon, Analysis of Surveyor 3 Materials and Photographs Returned by Apollo 12, 236-239, National Aeronautics and Space Administration.

Bunyard, G. B. (1973) Quantitative partial pressure measurements with the UTI precision gas analyzer, The UTI Journal of Quadrupole Mass Spectrometry, 1(1), 2-3, UTHE Technology International.

Carter, J. L. (1973) Morphology and chemistry of probable VLS (vapor-liquid-solid)-type of whisker structures and other features on the surface of breccia 15015,36, Proc. Fourth Lunar Sci. Conf., 1. 413-421, Pergamon Press.

Chapman, D. R. and Larson, H. K. (1963) On the lunar origin of tektites, J. Geophys. Res., 68, 4305-4358.

Clarke, R. S. Jr., Jarosewich, E., Mason, B., Nelen, J., Gomez, M., and Hyde, J. R. (1970) The Allende, Mexico, meteorite shower, Smithsonian Contrib. Earth Sci., 5, U. S. Govt. Printing Office.

Dawson, P. H. and Whetten, N. R. (1969) Mass Spectroscopy using RF quadrupole fields, Advan. Electron. Electron Phys., 27, 59-185.

De Maria, G., Balducci, G., Guido, M., and Piacente, V. (1971) Mass spectrometeric investigation of the vaporization process of Apollo 12 lunar samples, Proc. Second Lunar Sci. Conf., 2, 1367-1380, M. I. T. Press.

Derby, J. V. (1970) Ph. D. dissertation, University of Hawaii.

Drowart, J. and Goldfinger, P. (1967) Investigation of inorganic systems at high temperature by mass spectrometry, Angew. Chem., 6, 581-648.

Fincham, C. J. B. and Richardson, F. D. (1954) Viscosity and structure of molten silicates, Proc. Royal Soc. (London), A226, 423-435.

Fisher, D. E. (1971) Incorporation of argon in East Pacific basalts, Earth Planet. Sci. Lett., 12, 321-324.

Flaim, T. A. and Ownby, P. D. (1971) Observations on Bayard-Alpert ion gauge sensitivities to various gases, J. Vac. Sci. Techn., 8, 661-662.

Freeman, J. W., Hills, H. K., and Vondrak, R. R. (1972) Water vapor, whence comest thou? Proc. Third Lunar Sci. Conf., 3, 2217-2230.

Friedman, I. (1963) The physical properties and gas content of tektites, Tektites, J. A. O'Keefe (ed.), 130-136, University of Chicago Press.

Gast, P. W., Hubbard, N. J., and Wiesmann, H. (1970) Chemical composition and petrogenesis of basalts from Tranquility Base, Proc. Apollo 11 Lunar Sci. Conf., 2, 1143-1163, Pergamon Press.

Gibson, E. K. Jr. and Johnson, S. M. (1971) Thermal analysis-inorganic gas release studies of lunar samples, Proc. Second Lunar Sci. Conf., 2, 1351-1366, M. I. T. Press.

Gibson, E. K. Jr. and Hubbard, N. J. (1972) Thermal volatilization studies on lunar samples, Proc. Third Lunar Sci. Conf., 2, 2003-2014, M. I. T. Press.

Grimley, R. T. (1967) Mass spectrometry, The Characterization of High Temperature Vapors, J. L. Margrave (ed.), 195-243, John Wiley and Sons, Inc.

Hart, S. R. (1973) Submarine basalts from Kilauea Rift, Hawaii: nondependence of trace element composition on extrusion depth, Earth Planet Sci. Lett., 20, 201-203.

Hamilton, D. L., Burnham, C. W., and Osborn, E. F. (1964) The solubility of water and effects of oxygen fugacity and water content on crystallization in mafic magmas, J. Petrol., 5, 21-39.

Haughton, D. R., Roeder, P. L., and Skinner, B. J. (1974) Solubility of sulfur in mafic magmas, Econ. Geol., 69, 451-467.

Howard, K. A., Head, J. W., and Swann, G. A. (1972) Geology of Hadley Rille, Proc. Third Lunar Sci. Conf., 1, 1-14, M. I. T. Press.

Jedwab, J. (1973) Rare micron-size minerals in lunar fines, Proc. Fourth Lunar Sci. Conf., 1, 861-874, Pergamon Press.

Khitarov, N. I. and Kadik, A. A. (1973) Water and carbon dioxide in magmatic melts and peculiarities of the melting process, Contr. Mineral. Petrol., 41, 205-215.

Killingley, J. S. (1975) Ph. D. dissertation, University of Hawaii.

Knudsen, M. (1908) Die Gesetze der Molekularströmmung und der inneren Reibungsströmmung der Gase durch Röhren, Ann. Phys., 28, 75-130.

Lewis, G. N. and Randall, M. (1961) Thermodynamics, second ed. revised by K. S. Pitzer and L. Brewer, McGraw-Hill.

Lunar Sample Preliminary Examination Team (1972) The Apollo 15 samples: a preliminary description, Science, 175, 363-375.

Mason, B. and Melson, W. G. (1970) The Lunar Rocks, John Wiley and Sons, Inc.

Moore, J. G. (1965) Petrology of deep-sea basalt near Hawaii, Am. J. Sci., 263, 40-52.

Moore, J. G. and Calk, L. (1971) Sulfide spherules in vesicles of dredged pillow basalt, Am. Mineral., 56, 476-488.

Moore, W. J. (1962) Physical Chemistry, third ed., Prentice-Hall.

Muenow, D. W. (1973) Occurrence of volatile nitrides from silicates in low pressure, high temperature, reducing environments, Geochim. Cosmochim. Acta, 37, 2523-2528.

Nash, W. P. and Hausel, W. D. (1973) Partial pressures of oxygen, phosphorous and fluorine in some lunar lavas, Earth Planet. Sci. Lett., 20, 13-27.

Naughton, J. J., Derby, J. V., and Lewis, V. A. (1971) Vaporization from heated lunar samples and the investigation of lunar erosion by volatilized alkalis, Proc. Second Lunar Sci. Conf., 1, 449-457, M. I. T. Press.

Naughton, J. J., Hammond, D. A., Margolis, S. V., and Muenow, D. W. (1972) The nature and effect of the volatile cloud produced by volcanic and impact events on the Moon as derived from a terrestrial model, Proc. Third Lunar Sci. Conf., 2, 2015-2024, M. I. T. Press.

Nesmeyanov, An. N. (1963) Vapour Pressure of the Elements, 178, Table 76, Academic Press.

O'Hara, M. J., Biggar, G. M., Richardson, S. W., Ford, C. E., and Jamieson, B. G. (1970) The nature of seas, mascons, and the lunar interior in the light of experimental studies, Proc. Apollo 11 Lunar Sci. Conf., 1, 695-710, Pergamon Press.

Otvos, J. W. and Stevenson, D. P. (1956) Cross-sections of molecules for ionization by electrons, J. Am. Chem. Soc., 78, 546-551.

Rhodes, J. M. and Hubbard, N. J. (1973) Chemistry, classification and petrogenesis of Apollo 15 mare basalts, Proc. Fourth Lunar Sci. Conf., 2, 1127-1148, Pergamon Press.

Ringwood, A. E. and Essene, E. (1970) Petrogenesis of Apollo 11 basalts, internal constitution and origin of the Moon, Proc. Apollo 11 Lunar Sci. Conf., 1, 769-799, Pergamon Press.

Robie, R. A. and Waldbaum, D. R. (1968) Thermodynamic properties of minerals and related substances at 298.15° K (25.0° C) and one atmosphere (1.013 bars) pressure and at higher temperatures, U. S. Geol. Survey Bull. 1259.

Roboz, J. (1968) Introduction to Mass Spectrometry, John Wiley and Sons, Inc.

Roedder, E. and Weiblen, P. W. (1970) Lunar petrology of silicate melt inclusions, Apollo 11 rocks, Proc. Apollo 11 Lunar Sci. Conf., 1, 801-837, Pergamon Press.

Rüdenauer, F. G. (1972) A comparison between quadrupole and magnetic mass spectrometers for use in SIM, Vacuum, 11, 609-612.

Scarfe, C. M. (1973) Viscosity of basic magmas at varying pressure, Nature Phys. Sci., 241, 101-102.

Schnetzler, C. C. and Pinson, W. H. Jr. (1962) The chemical composition of tektites, Tektites, J. A. O'Keefe (ed.), 95-129, University of Chicago Press.

Simoneit, B. R., Christiansen, P. C., and Burlingame, A. L. (1973) Volatile element chemistry of selected lunar, meteoritic, and terrestrial samples, Proc. Fourth Lunar Sci. Conf., 2, 1635-1650, Pergamon Press.

Skinner, B. J. and Winchell, H. (1972) Mineralogical evidence for subsolidus vapor-phase transport of alkalis in lunar basalts, Proc. Third Lunar Sci. Conf., 1, 243-249, M. I. T. Press.

Smith, J. V., Anderson, A. T., Newton, R. C., Olsen, E. J., Wyllie, P. J., Crewe, A. V., Isaacson, M. S., and Johnson, D. (1970) Petrologic history of the Moon inferred from petrography, mineralogy, and petrogenesis of Apollo 11 rocks, Proc. Apollo 11 Lunar Sci. Conf., 1, 897-925, Pergamon Press.

Storey, W. C. (1973) Volatilization studies on a terrestrial basalt and their applicability to volatilization from the lunar surface, Nature Phys. Sci., 241, 154-157.

Stull, D. R. (ed.) (1965) JANAF Thermochemical Tables, NTIS doc. no. PB-168-370.

Taylor, S. R. (1973) Tektites: a post-Apollo view, Earth-Sci. Rev., 9, 101-123.

Turner, F. J. and Verhoogen, J. (1960) Igneous and Metamorphic petrology, second ed., McGraw-Hill.

Weill, D. F., McCallum, I. S., Bottinga, Y., Drake, M. J., and McKay, G. A. (1970) Petrology of a fine grained igneous rock from the Sea of Tranquillity, Science, 167, 635-638.

Wellman, T. R. (1970) Gaseous species in equilibrium with the Apollo 11 holocrystalline rocks during their crystallization, Nature, 225, 716-717.